Geoscientific
Model Development

The Flux-Anomaly-Forced Model Intercomparison Project (FAFMIP) contribution to CMIP6: investigation of sea-level and ocean climate change in response to CO$_2$ forcing

Jonathan M. Gregory[1,2], Nathaelle Bouttes[3], Stephen M. Griffies[4], Helmuth Haak[5], William J. Hurlin[4], Johann Jungclaus[5], Maxwell Kelley[6], Warren G. Lee[7], John Marshall[8], Anastasia Romanou[6], Oleg A. Saenko[7], Detlef Stammer[9], and Michael Winton[4]

[1]NCAS, University of Reading, Reading, UK
[2]Met Office Hadley Centre, Exeter, UK
[3]Laboratoire des Sciences du Climat et de l'Environnement, Institut Pierre Simon Laplace, Gif-sur-Yvette, France
[4]NOAA Geophysical Fluid Dynamics Laboratory, Princeton, USA
[5]Max Planck Institute for Meteorology, Hamburg, Germany
[6]Goddard Institute for Space Sciences, Columbia University, New York, USA
[7]Canadian Centre for Climate Modelling and Analysis, Victoria, British Columbia, Canada
[8]Department of Earth, Atmospheric and Planetary Sciences, Massachusetts Institute of Technology, Cambridge, USA
[9]Center for Earth System Research and Sustainability, University of Hamburg, Germany

Correspondence to: Jonathan M. Gregory (j.m.gregory@reading.ac.uk)

Abstract. The Flux-Anomaly-Forced Model Intercomparison Project (FAFMIP) aims to investigate the spread in simulations of sea-level and ocean climate change in response to CO$_2$ forcing by atmosphere–ocean general circulation models (AOGCMs). It is particularly motivated by the uncertainties in projections of ocean heat uptake, global-mean sea-level rise due to thermal expansion and the geographical patterns of sea-level change due to ocean density and circulation change. FAFMIP has three tier-1 experiments, in which prescribed surface flux perturbations of momentum, heat and freshwater respectively are applied to the ocean in separate AOGCM simulations. All other conditions are as in the pre-industrial control. The prescribed fields are typical of pattern and magnitude of changes in these fluxes projected by AOGCMs for doubled CO$_2$ concentration. Five groups have tested the experimental design with existing AOGCMs. Their results show diversity in the pattern and magnitude of changes, with some common qualitative features. Heat and water flux perturbation cause the dipole in sea-level change in the North Atlantic, while momentum and heat flux perturbation cause the gradient across the Antarctic Circumpolar Current. The Atlantic meridional overturning circulation (AMOC) declines in response to the heat flux perturbation, and there is a strong positive feedback on this effect due to the consequent cooling of sea-surface temperature in the North Atlantic, which enhances the local heat input to the ocean. The momentum and water flux perturbations do not substantially affect the AMOC. Heat is taken up largely as a passive tracer in the Southern Ocean, which is the region of greatest heat input, while the weakening of the AMOC causes redistribution of heat towards lower latitudes. Future analysis of these and other phenomena with the wider range of CMIP6 FAFMIP AOGCMs will benefit from new diagnostics of temperature and salinity tendencies, which will enable investigation of the model spread in behaviour in terms of physical processes as formulated in the models.

1   Introduction

Atmosphere–ocean general circulation models (AOGCMs) are widely used for projections of future sea-level change (e.g. Church et al., 2013; Slangen et al., 2014). On the basis of AOGCM results contributed to the Coupled Model Intercomparison Project Phase 5 (CMIP5), global-mean sea-level rise (GMSLR) of 0.32–0.63 m (5–95 %, median 0.47 m) is projected by 2081–2100 under the mid-range RCP4.5 scenario considered in the Fifth Assessment Report of the Intergovernmental Panel on Climate Change (IPCC) (Yin, 2012; Church et al., 2013). Of this, 0.14–0.23 m (median 0.19 m) is the thermosteric contribution, due to expansion of seawater as the ocean takes up heat, representing 30–50 % of the total. Other contributions to GMSLR are due mostly to loss of land ice. Glaciers worldwide give 15–40 % of the total. The median projected contributions from the Greenland and Antarctic ice sheets are smaller, although the latter is the largest source of uncertainty.

The range of the thermosteric contribution (hereafter denoted h_θ) also represents a substantial uncertainty in projections of GMSLR. It arises partly from differences among models in climate sensitivity, determined by surface and atmospheric responses to radiative forcing, and partly from differences in the ocean processes which transport heat from the surface and redistribute it in the interior of the ocean (Kuhlbrodt and Gregory, 2012; Hallberg et al., 2013; Melet and Meyssignac, 2015). The three-dimensional distribution of additional heat within the ocean affects h_θ because of the dependence of thermal expansivity on temperature and pressure, quantified by the "expansion efficiency of heat" (Russell et al., 2000; Griffies and Greatbatch, 2012; Kuhlbrodt and Gregory, 2012; Griffies et al., 2014), the ratio of h_θ to the global ocean increase in heat content. From CMIP5 results, this ratio is 0.12 m YJ^{-1} (1 YJ $\equiv 10^{24}$ J), with a 90 % confidence interval of 0.10–0.14 m YJ^{-1} (Lorbacher et al., 2015), indicating that there is an uncertainty in the h_θ that results from a given increase in ocean heat content. By contrast, redistribution of the salt content of the ocean makes a negligible contribution to GMSLR or its uncertainty.

Sea-level change is not expected to be globally uniform. Changes in ocean circulation, temperature and salinity (and hence density) alter dynamic sea level $\zeta(\boldsymbol{x}, t)$, where $\boldsymbol{x}$ is location and t time. This quantity is defined as

$$\zeta(\boldsymbol{x}, t) \equiv \eta(\boldsymbol{x}, t) - \overline{\eta(\boldsymbol{x}, t)}, \qquad (1)$$

where η is sea-surface height relative to a surface on which the geopotential has a uniform and constant value, and the overline indicates the mean over the ocean area, so $\bar{\zeta} = 0$ by construction. Hence

$$\Delta\eta = \Delta\zeta + \Delta\bar{\eta}, \qquad (2)$$

in which the last term is GMSLR. That is, the local change in sea level $\Delta\eta$ has contributions from GMSLR and from change in dynamic sea level $\Delta\zeta$. The spatial standard deviation of the CMIP5 model mean $\Delta\zeta$ is about 30 % of the model-mean global-mean thermosteric contribution h_θ (Fig. 1a).

There is a substantial model spread in $\Delta\zeta$, although in some regions, notably the Arctic, the model spread is smaller than in the previous phases of CMIP considered by earlier IPCC reports (Yin, 2012; Bouttes et al., 2012; Church et al., 2013; Slangen et al., 2014). Nonetheless, the CMIP5 RCP4.5 local spread in the pattern, measured by the ensemble standard deviation of $\zeta(\boldsymbol{x})$, is 30 % on average of the model mean h_θ, and for example it exceeds 100 % in the North Atlantic (Fig. 1b).

There are three features of $\Delta\zeta$ that the models have in common (Fig. 1a) (Gregory et al., 2001; Church et al., 2001; Lowe and Gregory, 2006; Landerer et al., 2007; Meehl et al., 2007; Yin et al., 2010; Pardaens et al., 2011; Yin, 2012; Church et al., 2013; Slangen et al., 2014; Bouttes and Gregory, 2014): (i) a meridional contrast between a band of positive change to the north of the Antarctic Circumpolar Current (ACC) and a band of negative change to the south, (ii) a meridional dipole in the North Atlantic, also positive to the north and negative to the south and (iii) positive $\Delta\zeta$ in the Arctic. Although these qualitative features are robustly predicted, the affected regions have the largest model spread in $\Delta\zeta$.

The Southern Ocean feature results both from changes to the surface heat flux and from an intensification and southward shift of the westerly wind stress, which strengthens the Ekman drift and tends to tilt the isopycnals (Mikolajewicz and Voss, 2000; Lowe and Gregory, 2006; Landerer et al., 2007; Frankcombe et al., 2013; Bouttes and Gregory, 2014; Kuhlbrodt et al., 2015; Saenko et al., 2015; Marshall et al., 2015). Eddies tend to oppose the latter effect by removing available potential energy, thus partly compensating for the effect of wind-stress change in $\Delta\zeta$, and limiting the sensitivity of the circumpolar circulation to wind-stress change (Hallberg and Gnanadesikan, 2006; Böning et al., 2008; Farneti et al., 2010, 2015; Downes and Hogg, 2013). Most AOGCMs used for multidecadal simulations do not resolve ocean eddies at high latitudes, so their results will depend on their parametrisations of eddy advection on isoneutral surfaces (e.g. Gent and McWilliams, 1990; Griffies, 1998).

The North Atlantic feature in $\Delta\zeta$ is caused by increased ocean buoyancy at high latitudes under CO_2 forcing (Bouttes et al., 2014). The buoyancy increase is due to reduced heat loss and increased precipitation. As well as tending to raise sea level, it leads to a reduction of the Atlantic meridional overturning circulation (AMOC), by 0–50 % by 2100 in CMIP5 AOGCMs, depending on model and scenario (Collins et al., 2013). The circulation change causes a redistribution of properties, giving a negative $\Delta\zeta$ in the subtropical North Atlantic gyre. The enhanced sea-level rise in the Arctic has been attributed to increased buoyancy from re-
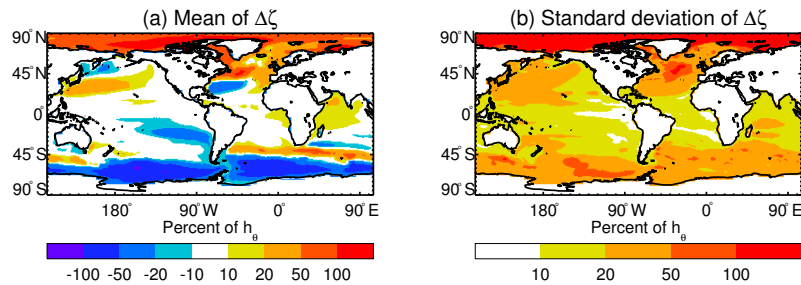
Figure 1. (a) Ensemble mean and **(b)** ensemble standard deviation of CMIP5 AOGCMs for the projected change $\Delta\zeta$ in ocean dynamic sea level for 2081–2100 with respect to 1986–2005 under the mid-range scenario RCP4.5, expressed as percentages of ensemble-mean global-mean sea-level rise h_θ due to thermal expansion for the same scenario.

duction of salinity (Meehl et al., 2007; Griffies et al., 2014), consistent with greater precipitation and river inflow.

Bouttes et al. (2012) investigated how much of the model spread in CMIP5 $\Delta\zeta$ was caused by the AOGCMs' different projections of surface momentum flux change in response to increasing CO_2. They did so by computing the field of surface wind-stress change simulated for doubled CO_2 by each CMIP5 AOGCM, and imposed these fields as perturbations in a set of experiments (one for each CMIP5 model) with the FAMOUS AOGCM (Smith et al., 2008), which is a low-resolution and consequently relatively inexpensive version of HadCM3. Bouttes et al. (2014) carried out a corresponding study for surface heat flux and freshwater flux changes. These studies show that part of the model spread in $\Delta\zeta$ arises from the spread of surface flux changes predicted by AOGCMs (Bouttes and Gregory, 2014), especially regarding the amplitude of the changes.

However, the FAMOUS experiments tend to be similar in their patterns of change; they do not reproduce the diversity of patterns of $\Delta\zeta$ in the AOGCMs supplying the surface flux perturbations. The unexplained model spread in patterns and amplitude of $\Delta\zeta$ must arise from dependence on the ocean model formulation and unperturbed state. These aspects are so far largely unexplored and need further constraint, but comparisons of the ocean response in AOGCMs are complicated by their different predictions of changes to surface fluxes experienced by the ocean.

Consequently, the Flux-Anomaly-Forced Model Intercomparison Project (FAFMIP) was proposed to isolate the ocean uncertainty, by comparing results from AOGCM experiments in which model-independent surface flux perturbations are imposed on the ocean. FAFMIP is a component of CMIP6, the phase of CMIP which is now beginning (Eyring et al., 2016). At the time of writing there were 10 modelling groups planning to run FAFMIP experiments as part of their contributions to CMIP6, namely ACCESS (Australia), CCCma/CanESM (Canada), CNRM/CERFACS (France), GFDL (USA), GISS (USA), IPSL (France), MIROC (Japan), MPI-ESM (Germany), MRI (Japan) and UKESM (UK). FAFMIP is an element of the science plan for the World Cli-

mate Research Programme (WCRP) Grand Challenge on regional sea-level change and coastal impacts.

The AOGCMs participating in FAFMIP will include new three-dimensional ocean diagnostics of the rates of change of temperature and salinity due to the individual processes which transport heat and salt within the ocean (resolved advection, dianeutral mixing, etc.). Such ocean process-based diagnostics have previously been included in only a small number of models (e.g. Gregory, 2000; Huang et al., 2003; Morrison et al., 2013, 2016; Palter et al., 2014; Exarchou et al., 2015; Griffies et al., 2015; Kuhlbrodt et al., 2015), and cannot be estimated accurately from other archived data. The FAFMIP experiments and diagnostics will for the first time permit us to attribute differences in the ocean among a wide range of models in the unperturbed state and in CO_2-forced climate change to particular processes and aspects of model formulation.

The FAFMIP experiments will provide information on the sensitivity of the AMOC to buoyancy forcing of the magnitude and pattern of that predicted for CO_2 forcing, and will support investigation of the correlation between ocean heat uptake efficiency and the magnitude of the AMOC (Rugenstein et al., 2013; Winton et al., 2014; Kostov et al., 2014). The application of common perturbations to surface fluxes in FAFMIP will provide information about the ocean's role in determining patterns of sea-surface temperature change worldwide (of relevance to the Grand Challenge on clouds, circulation and climate sensitivity). Similarly the results will be of relevance to studies of subsurface ocean temperature change in the vicinity of Greenland and Antarctic ice shelves (Yin et al., 2011; Spence et al., 2014; Stewart and Thompson, 2015), where warming may promote basal melting of ice shelves and consequent sea-level rise through the effect on ice-sheet dynamics (of relevance to the Grand Challenge on melting ice and global consequences, as well as sea level).

FAFMIP will thus help with understanding and accounting for the spread in simulated ocean responses in general to changes in surface fluxes resulting from CO_2 forcing. In the next section we describe the design of FAFMIP, and in the following section we present preliminary results from exper-

iments that have been carried out in a small number of existing AOGCMs to test the design.

2   Design

The aim of the FAFMIP tier-1 experiments is to study the response of the ocean to the changes in its surface fluxes caused by CO_2-forced climate change, in particular regarding sea level, ocean heat uptake and ocean circulation. The design allows the effects of changes in surface fluxes of momentum, heat and freshwater to be separated, and aims to simplify the analysis of the diversity of ocean response by imposing the same changes in surface fluxes in every AOGCM. This is by contrast with CO_2-forced climate-change experiments, such as 1pctCO2, in which the surface fluxes are model-dependent.

2.1   AOGCMs and surface flux perturbations

The atmosphere and ocean are a tightly coupled system, especially through the interaction of surface heat flux and sea surface temperature (SST). It typically requires millennia of "spin-up" integration of an AOGCM with constant atmospheric composition (the pre-industrial control experiment, denoted "piControl") to reach an approximately steady state in the deep ocean, owing to its large heat capacity and weak thermal connection to the surface (Danabasoglu, 2004; Stouffer, 2004; Sen Gupta and England, 2004; Banks et al., 2007; Sen Gupta et al., 2013). Even then, a small "climate drift" may persist. Experiments have been done successfully in which surface fluxes from one climate state of an AOGCM are transplanted into a simulation of another climate state of the same AOGCM (Mikolajewicz and Voss, 2000; Gregory et al., 2005). However, if one replaces AOGCM ocean surface fluxes with real-world estimates or with fluxes diagnosed from *another* model, a large climate drift will result, because they will not be consistent with the AOGCM's own surface climate. Therefore the FAFMIP experiments instead impose *perturbations*, added to the surface fluxes that are computed within the AOGCM from the state of the system (Lowe and Gregory, 2006; Bouttes and Gregory, 2014), technically like the flux adjustment that was formerly used in AOGCMs (Sausen et al., 1988) but with a different purpose.

The principle of the FAFMIP experiments is that the ocean should respond as it does during an AOGCM climate-change experiment, as nearly as possible, including interactively simulated atmosphere–ocean feedbacks and unforced variability. The FAFMIP design contrasts with that of studies using (uncoupled) ocean GCMs, such as the CORE project (e.g. Griffies et al., 2014), in which bulk formulae are used to compute fluxes from prescribed observationally derived surface climate variables, and the experiments of Marshall et al. (2015), with a prescribed geographically uniform surface heat flux perturbation and feedback parameter.

Those approaches yield valuable and complementary information about the response of the ocean to perturbations, but are less like the AOGCM projections whose uncertainty we aim to investigate.

2.2   Deriving the surface flux perturbations

Climate-change projection is concerned mostly with scenarios of radiative forcing increasing on decadal timescales. The idealised scenario called "1pctCO2" in CMIP6 (and CMIP5), beginning from a piControl state and with atmospheric CO_2 concentration increasing at $1\%\,year^{-1}$, is commonly taken to be indicative of anthropogenic climate change expected during this century. It is a useful benchmark because it has been studied since the first AOGCM experiments in the early 1990s, while the more policy-specific scenarios, involving emissions of many species and complicated time profiles of forcing, have been revised several times. The transient climate response (TCR) is likewise used for convenient comparison of the magnitude of climate change, and is defined (Cubasch et al., 2001) as the difference from piControl of the time-mean global-mean surface air temperature during years 61–80 of 1pctCO2, centred around the time (70 years) at which CO_2 reaches double its piControl concentration.

For consistency with this conventional choice, we obtain the surface flux perturbations for FAFMIP from years 61–80 of CMIP5 1pctCO2 experiments. In experiments with time-dependent forcing scenarios, the geographical pattern of sea-level change is fairly constant in time, but has increasing amplitude (Perrette et al., 2013; Bilbao et al., 2015), as is often assumed for surface air temperature and other surface quantities (Santer et al., 1990; Huntingford et al., 2000; Collins et al., 2013). To investigate the causes of the patterns we therefore do not need to include interannual variation in the surface flux perturbations. In the FAFMIP experiments, the perturbations are imposed from the start and held constant (apart from their seasonal cycle). Tests with the FAMOUS AOGCM indicated that similar geographical patterns of sea-level change result from time-dependent flux perturbations from 1pctCO2 experiments as from the time-independent FAFMIP flux perturbations.

The surface flux perturbations are derived from a set of 13 CMIP5 AOGCMs for which all the required diagnostics are available, namely CNRM-CM5, CSIRO-Mk3-6-0, CanESM2, GFDL-ESM2G, HadGEM2-ES, MIROC-ESM, MIROC5, MPI-ESM-LR, MPI-ESM-MR, MPI-ESM-P, MRI-CGCM3, NorESM1-ME and NorESM1-M. More AOGCMs could have been included for some types of perturbation, but it was decided to use this restricted but consistent set of AOGCMs for all perturbations, in order to permit comparison with the model-mean change in sea level and other quantities from the same set of AOGCMs. The diversity in the surface flux changes from the individual CMIP5 AOGCMs is illustrated by Bouttes and Gregory (2014, their Fig. 2). For each of four types of surface flux (zonal and
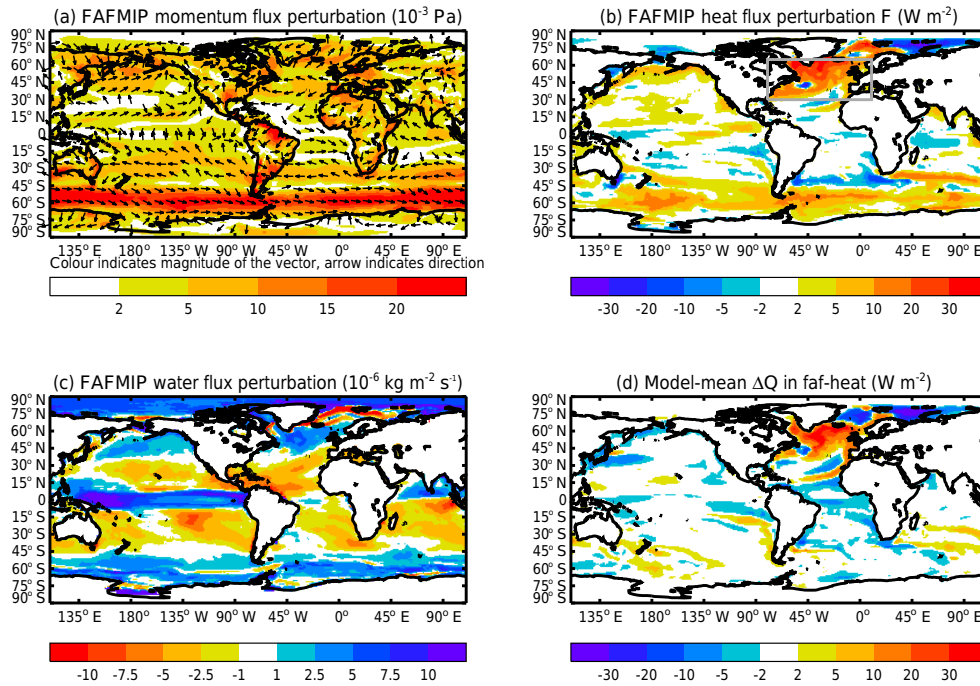
Figure 2. Annual-mean FAFMIP surface flux perturbations of **(a)** momentum, **(b)** heat, **(c)** water; **(d)** shows the model-mean change in the surface heat flux Q into the seawater in the time mean of the final decade of the faf-heat experiment relative to the control, not including the imposed heat flux perturbation F. The ocean area average of **(b)** is $1.86\,\mathrm{W\,m^{-2}}$, of **(c)** $0.072 \times 10^{-6}\,\mathrm{kg\,m^{-2}\,s^{-1}}$ and of **(d)** $0.07\,\mathrm{W\,m^{-2}}$. The grey box in **(b)** is the North Atlantic region to which we refer in Sect. 3.1.

meridional momentum, heat and freshwater, Sect. 2.3), a difference field for each model is computed between the climatological monthly time means of years 61–80 of 1pctCO2, using the first member in cases of an ensemble, and of the corresponding 20 years of piControl, then interpolated to a common 1° latitude–longitude grid. Finally, the mean of the models is calculated.

The resulting model-mean fields for use in the FAFMIP experiments are stored in CF-netCDF files at http://www.fafmip.org. They are monthly means, which can be regarded as applying at the middle of the month, and it is recommended to interpolate linearly between them in time to obtain updates at the atmosphere–ocean coupling interval. Horizontal interpolation to the required ocean model grid may not exactly preserve the global integral but the differences are not likely to be important.

2.3 Experiments

The FAFMIP experiments (Table 1) branch from piControl and have piControl boundary conditions (atmospheric composition, solar irradiance, land surface, etc.). The best point to branch would be the same point as the 1pctCO2 experiment, with which FAFMIP results may be compared. The experiments are proposed as 70 years long, but because a large perturbation is switched on instantaneously at the start, useful results could be obtained from shorter integrations

Table 1. FAFMIP experiments.

Name	Ocean surface flux perturbation
Tier 1	
faf-stress	Zonal and meridional momentum
faf-heat	Heat
faf-water	Freshwater
Tier 2	
faf-all	All from faf-stress, faf-heat and faf-water
faf-passiveheat	Heat as in faf-heat, but added as a passive tracer

The process-based tendency diagnostics (Sect. 2.6) should be included in the FAFMIP experiments and in the DECK abrupt4xCO2 and 1pctCO2 and the corresponding section of piControl. The faf-passiveheat experiment is identical to piControl except for the inclusion of the added heat tracer, so a separate integration may not be needed.

of computationally expensive models. During the first several decades of a typical AOGCM 1pctCO2 integration, the global-mean surface air temperature and net heat flux into the ocean rise roughly linearly in time (e.g. Gregory and Mitchell, 1997). The flux perturbations in FAFMIP integrations are typical of year 70 of a 1pctCO2 experiment. Therefore 70 years of a FAFMIP integration will apply roughly the same time-integral forcing to the ocean as $70\sqrt{2} \simeq 100$ years of a 1pctCO2 integration.

Three experiments are required for participation in FAFMIP (tier 1):

In *faf-stress* we impose a perturbation in surface zonal and meridional momentum flux, i.e. wind stress (Fig. 2a), created from the CMIP5 diagnostics of surface downward fluxes of eastward (`tauu`) and northward (`tauv`) momentum. Its dominant feature is the increase in westerly wind stress in the Southern Ocean. The stress perturbation is added to the momentum balance of the ocean water surface. For instance, the modified equation of motion of the top layer of a hydrostatic ocean model is

$$\frac{\partial \boldsymbol{u}_h}{\partial t} = -(\boldsymbol{u} \cdot \nabla)\boldsymbol{u}_h - \frac{1}{\rho}\nabla_h p - \boldsymbol{f} \times \boldsymbol{u}_h + \frac{1}{\rho}\mathbf{R}$$
$$+ \frac{1}{m_t}(\boldsymbol{\tau}_w + \boldsymbol{\tau}_i + \mathbf{S}), \tag{3}$$

where $\boldsymbol{u}$ is velocity, subscript h indicates the horizontal part, t is time, p hydrostatic pressure, ρ density, $\boldsymbol{f}$ the product of the Coriolis parameter and the vertical unit vector, $\mathbf{R}$ the vertical and horizontal convergence of horizontal momentum (in $\mathrm{N\,m^{-3}}$) due to subgridscale processes (including the shear stress which conveys the surface momentum fluxes into the subsurface), $\boldsymbol{\tau}_w$ the wind stress, $\boldsymbol{\tau}_i$ the stress exerted by sea ice, $\mathbf{S}$ the faf-stress momentum flux perturbation (in Pa, like $\boldsymbol{\tau}_{w,i}$), and m_t is the mass per unit area of the top layer of the model, to which the surface momentum fluxes are applied. No perturbation should be made directly to any turbulent mixing scheme that depends on the wind stress, nor to the sea-ice momentum balance, although both of these could be indirectly influenced since $\boldsymbol{\tau}_w$ and $\boldsymbol{\tau}_i$ may be affected by changes in the surface $\boldsymbol{u}_h$.

In *faf-heat* we impose a perturbation on the heat flux into the seawater surface (Fig. 2b), created from the CMIP5 diagnostic of surface downward heat flux in seawater (`hfds`), i.e. the sum of net downward radiative fluxes, sensible and latent heat fluxes to the atmosphere, and heat fluxes between sea ice and seawater. The heat flux perturbation is strongly positive in the North Atlantic and in the Southern Ocean. Imposing a heat flux perturbation in an AOGCM by adding it to the ocean surface layer alters the SST and thus modifies the surface heat flux so as to oppose the perturbation. Such a strong negative feedback does not occur with the momentum flux, which is only fairly weakly affected by the seawater surface velocity, nor with the freshwater flux, which does not depend on the surface salinity. The method for implementing faf-heat is the one used by Bouttes et al. (2014), described below and compared with alternatives (Sect. 2.4); it is intended to avoid this negative feedback, but permits feedbacks due to ocean circulation change. The method allows us to partition ocean temperature change between the effects of local addition of heat and changing heat transports, using three-dimensional ocean tracer fields of "added heat" and "redistributed heat" (Sect. 2.5).

In *faf-water* we impose a perturbation on the freshwater flux into the seawater surface (Fig. 2c), created from the CMIP5 diagnostic of water flux into seawater (`wfo`), i.e. the sum of precipitation, evaporation, river inflow and water
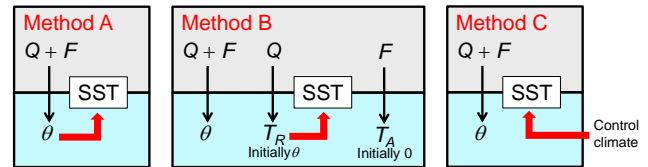
Figure 3. The three methods for treating the surface heat flux in faf-heat and faf-all, described in Sect. 2.4. The methods differ regarding the SST which is used to calculate the net surface heat flux Q from the atmosphere and sea ice into the ocean water. In method A it is obtained from the top-layer ocean temperature θ as usual in an AOGCM, in method B from the redistributed heat tracer T_R, and in method C the SST and sea ice are prescribed from the climatology of the AOGCM control experiment.

fluxes between floating ice (sea ice and icebergs) and seawater. Its pattern is dominated by that of precipitation change, being positive near the Equator and at mid- to high latitudes, and negative in the subtropics. In the Arctic there is also increased water input from river inflow, and a pronounced band of reduced water input from melting along the sea-ice margin, which retreats to higher latitude in the $2 \times CO_2$ climate.

Two further experiments are recommended (tier 2):

In *faf-all* the surface flux perturbations of momentum, heat and freshwater are simultaneously applied, using the same method for heat as in the faf-heat experiment. By comparison with the tier-1 experiments, faf-all will be used to quantify non-linearities in the combination of the effects of the perturbations. If the combination is linear, the ocean response to CO_2 forcing may be interpreted as the sum of the effects.

In *faf-passiveheat* a surface flux equal to the surface heat flux perturbation of the faf-heat experiment is applied instead to a passive "added heat" tracer (Sect. 2.4), initialised to zero. This tracer does not affect the model evolution, so the experiment is equivalent to piControl, with an extra diagnostic tracer. Comparison of faf-passiveheat with faf-heat will allow the effect on the distribution of the added heat from changes in ocean heat transport to be assessed, because these changes do not occur in faf-passiveheat.

Apart from the partial suppression of changes in surface heat flux in faf-heat (discussed above and in the next section), the surface fluxes of momentum, heat and freshwater are computed as usual in the AOGCM. In general they will all differ from the piControl state because of climate change caused by applying the perturbation fluxes to the ocean. In models where the sensible heat content of ocean surface water fluxes (precipitation, evaporation and runoff) is considered, faf-water will in effect also impose a small heat flux perturbation. Further technical notes on the implementation of each of the experiments can be found at http://www.fafmip.org.

2.4 Treatment of the surface heat flux

In this section we consider methods for treating the surface heat flux in faf-heat and faf-all. The methods differ regarding the calculation of the net surface heat flux Q from the atmosphere and sea ice into the ocean water computed by the AOGCM from its prognostic state. We refer to the method used by Bouttes et al. (2014) as "B", and compare it with two alternatives, referred to as "A" and "C", with experiments using the HadCM3 AOGCM (Table 2). The three methods are summarised and compared in Fig. 3.

In all methods, the net surface heat flux applied to the top-layer θ in faf-heat is $Q + F$, where F is the FAFMIP prescribed heat flux perturbation, and θ stands for the ocean model temperature field – either potential or conservative, whichever is used in the equation of state to compute density. Let us write $Q = Q_c$ for the piControl experiment and $Q = Q_p$ for faf-heat. In both experiments there is unforced interannual variation in Q, while the prescribed F has no interannual variation (although it does have a seasonal cycle). The climatological mean difference in net surface heat flux between the experiments is

$$Q_+ = \langle Q_p \rangle + F - \langle Q_c \rangle = \langle \Delta Q \rangle + F, \tag{4}$$

where $\Delta Q = Q_p - Q_c$ and $\langle \rangle$ indicates a climatological time mean. The aim is that Q_+, the difference in surface heat flux between faf-heat and piControl, should equal F, the CMIP5 model-mean difference in surface heat flux between the $2 \times CO_2$ climate (in 1pctCO2) and piControl.

In *method A*, the heat flux perturbation F is added to the top layer in the prognostic equation for θ, and the heat fluxes between atmosphere, sea ice and ocean are calculated as usual in the AOGCM. Since $F > 0$ in large regions and in the global mean (Fig. 2b), surface air temperature generally rises, causing a negative change ΔQ in the net surface heat flux into the ocean. This change opposes F, so $\overline{Q_+} < \overline{F}$ (Eq. 4; the overline indicates the mean over the ocean area as before). In the HadCM3 experiment with method A, global-mean surface air temperature rises by 0.8 K (Fig. 4b), and the ocean area mean $\langle \overline{\Delta Q} \rangle = -0.81\,\mathrm{W\,m^{-2}}$, while $\overline{F} = 1.86\,\mathrm{W\,m^{-2}}$. Thus only $1 + \langle \overline{\Delta Q} \rangle / \overline{F} = 56\,\%$ of the heat flux perturbation is added to the ocean. Locally $\langle \Delta Q \rangle$ is generally of opposite sign to F (compare Figs. 2b and 4a), as expected, and it is of particularly large magnitude in the North Atlantic.

In *method B* (further discussed in Sect. 2.5), we introduce a passive tracer T_R, i.e. one which does not affect density. It is initialised to θ at the start of the experiment, and subsequently transported by all the same processes as θ. The model's surface heat flux Q is applied to T_R as well as to θ, but T_R does not feel the heat flux perturbation F. The critical difference from method A is that the SST for computing Q is supplied by T_R instead of θ, and is therefore not directly affected by F. This mitigates the feedback in which ΔQ opposes F. Similarly T_R is used instead of θ in calculations

of the heat fluxes between the ocean and sea ice, so that F does not directly affect the sea-ice heat budget. If $F = 0$, T_R evolves like θ and the climate will be the same as in piControl. Method B is more complicated than method A because of the need for T_R and small modifications to the coupling to atmosphere and sea-ice submodels. However, extra tracers are a standard mechanism in many OGCMs because of the role in ocean biogeochemistry and for diagnostics such as idealised age and chemical species.

In the HadCM3 experiment with method B, the change in global-mean surface air temperature is prevented (Fig. 4b), and ocean area mean $\langle \overline{\Delta Q} \rangle = +0.037\,\mathrm{W\,m^{-2}}$, so 102 % of the heat flux perturbation is added to the ocean, causing a greater increase in ocean heat content than in method A (Fig. 4d). Locally ΔQ is no longer markedly anticorrelated with F (compare Figs. 2b and 4c). Whereas method A puts less heat than the intended F into the North Atlantic, method B puts more than intended, as a result of the weakening of the AMOC caused by the heat flux perturbation. This change in ocean circulation reduces the advective heat convergence to the North Atlantic. In consequence, in the unmodified AOGCM, the regional SST tends to cool, and the surface heat flux into the ocean tends to increase (although there is still a net heat flux out of the ocean in the majority of the region). Winton et al. (2013) show that about one-third of the reduction in heat convergence may thus be offset by a further increase in surface heat flux. This feedback mechanism is presumably at work in the CMIP5 1pctCO2 experiments from which the faf-heat F has been calculated, and F therefore includes an enhancement due to reduction of advective heat convergence in those models. But the mechanism operates in faf-heat as well, because weakening of the AMOC will reduce the convergence of T_R, from which Q is calculated. Hence this phenomenon is exaggerated in method B, making Q_+ larger than intended. The change in advection also means that Q_+ does not have the intended geographical distribution.

In *method C* for faf-heat, the AOGCM uses climatological monthly time means of SST and sea ice from piControl, instead of the prognostic state of the system, to compute the ocean surface heat flux Q. The sea-surface conditions evolve in response to F in the ocean submodel, but these changes do not affect the atmosphere submodel. Because this method suppresses the interaction between surface climate and atmosphere, an ocean climate drift results even if $F = 0$.

In our HadCM3 test of method C, the surface climate for $F = 0$ stabilises within about 100 years; this timescale is no doubt model-dependent. The ocean area-mean SST is 1.4 K warmer than in the HadCM3 control, with cooling of more than 2 K in the North Atlantic, although the AMOC is unaffected in strength, and warming of more than 2 K in low latitudes. The sea-surface conditions applying to the ocean and atmosphere are therefore markedly different, since the latter is prescribed unchanged from the control. In the global mean the ocean warming penetrates to about 500 m depth,
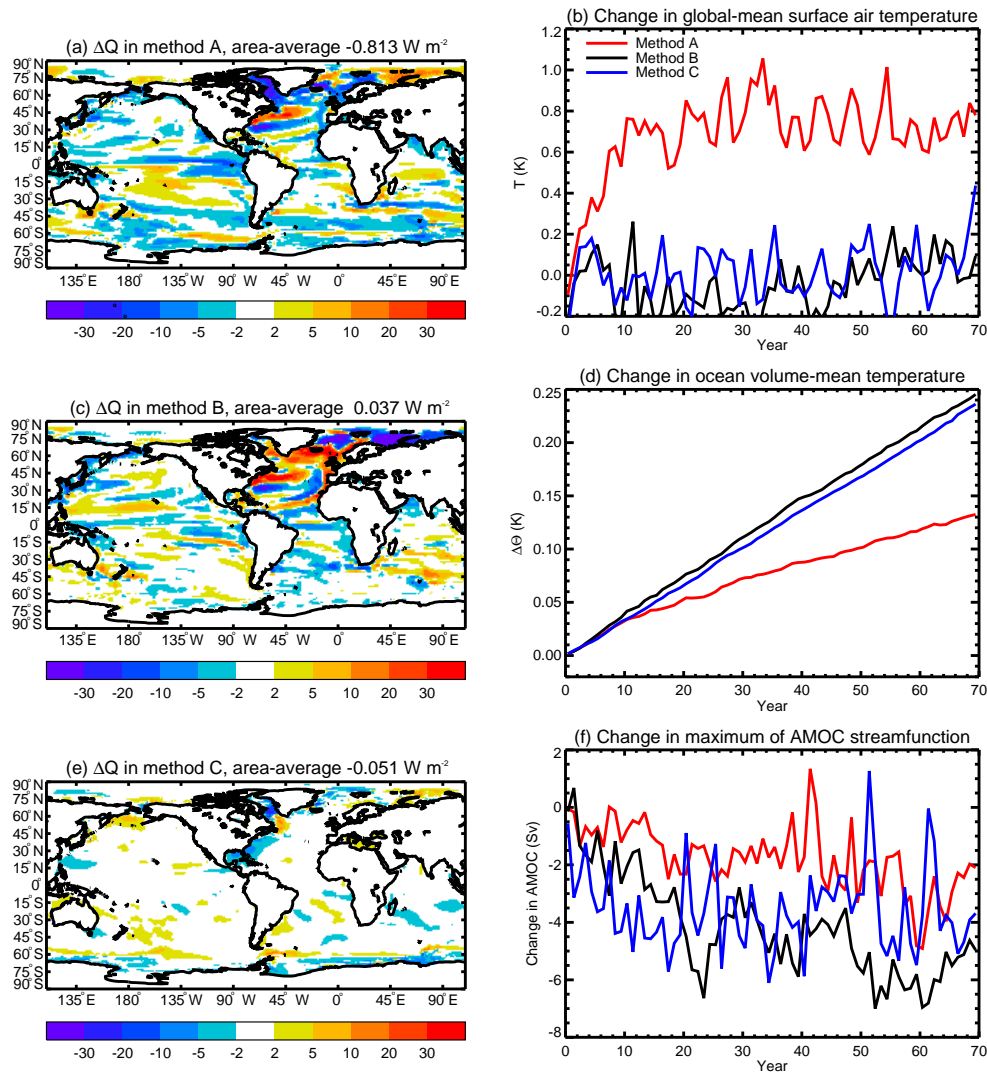
Figure 4. (a, c, e) The change ΔQ $(\mathrm{W\,m^{-2}})$ in the surface heat flux into seawater in the time mean of the 70 years of the HadCM3 faf-heat experiment relative to the control, not including the imposed heat flux perturbation, in methods A, B and C; **(b, d, f)** annual time series of the change relative to control in global-mean surface air temperature ΔT, ocean volume-mean temperature and the maximum of AMOC streamfunction, with the three methods. In method A the heat flux perturbation F causes ΔT to increase **(b)**, giving a negative feedback on ocean heat uptake **(d)**; this effect is prevented in the other methods, as discussed in Sect. 2.4.

with both cooling and warming of more than 1 K in magnitude at greater depths in high northern latitudes. The ocean area-mean surface salinity increases by about 0.5 PSU. These changes are comparable in magnitude with those that result from $2 \times CO_2$ forcing, meaning that for method C, unlike method B, a new control experiment with $F = 0$ is required in parallel to faf-heat to evaluate the response to the perturbative F.

In method C, the effect of F on ΔQ via SST is eliminated, and Q_+ is close to F. In HadCM3 with method C 97 % of the global mean F is added to the ocean, whose heat content therefore increases slightly less than in method B (Fig. 4d). However, ΔQ is not zero everywhere (Fig. 4e), be-

cause the faf-heat and corresponding piControl integrations have different unforced variability in the atmosphere, and because changes in ocean surface velocity are seen by the atmosphere.

Since method C applies the heat flux perturbation accurately to the North Atlantic, without allowing the strong local feedback on Q, its simulation of the AMOC decline may give the best estimate of the response to the intended F. Compared with method C, the AMOC weakening is too small in method A and too large in method B (Fig. 4f). We note that when Bouttes et al. (2014, their Fig. 5) applied surface heat flux perturbations from CMIP5 AOGCMs to the FAMOUS AOGCM using method B, the weakening of the AMOC in

Table 2. AOGCMs used for FAFMIP preliminary experiments.

Name	L	Ocean horizontal grid	References	F	ΔQ		ΔAMOC	
					G	NA	FAF	1pct
HadCM3	20	1.25° longitude–latitude	Gordon et al. (2000)	1.80	−0.04	0.45	−5.6	−2.3
CanESM2	40	1.4° longitude × ∼ 0.93° latitude	Yang and Saenko (2012) with small updates*	1.90	0.05	0.53	−7.3	−2.5
GFDL-ESM2M	50	1° tripolar, refined at low latitude to $\frac{1}{3}$° in tropics	Dunne et al. (2012)	1.86	0.10	0.45	−12.0	−6.8
MPI-ESM-LR	40	0.13–1.65° curvilinear	Giorgetta et al. (2013) with small updates	1.97	0.15	0.51	−9.5	−3.8
GISS-E2-R-CC	32	1.25° longitude × 1.0° latitude	Schmidt et al. (2006)					

* The most important update is the use of a baroclinicity-dependent formulation for the eddy transfer coefficient in the scheme of Gent and McWilliams (1990).
The column marked "L" indicates the number of ocean model levels. The column marked "F" is the ocean area-mean surface heat flux perturbation (W m^{-2}) in faf-heat. The columns marked "ΔQ" indicate the time-mean area-mean difference in the surface heat flux (W m^{-2}) computed by the AOGCM between faf-heat and the control, "G" for the global ocean area, "NA" for the North Atlantic area marked in Fig. 2b. The columns marked "ΔAMOC" indicate the change in the AMOC (Sv), "FAF" for the time mean of the last decade of faf-heat compared with its control, "1pctCO2" for the time mean of years 61–80 in 1pctCO2 compared with piControl in CMIP5 results with the same model.

FAMOUS was not systematically stronger than in the CMIP5 AOGCMs. This indicates that strength of advection feedback on Q is model-dependent, as we also see later (Sect. 3.1).

Although method C is arguably most accurate, it has the disadvantages that it is more computationally expensive (because of the need for a new control integration), the ocean climate state is different from the unmodified AOGCM whose response we wish to investigate and the physical interaction between atmosphere and ocean is unrealistically suppressed, including feedbacks which could be of interest. We therefore adopt method B for faf-heat.

2.5 Added and redistributed heat

Changes in θ in method B can be partitioned into those due to modified tracer transport processes (due to change in circulation, diffusion, etc.) and those due to added heat (following Banks and Gregory, 2006; Xie and Vallis, 2012). We are interested in the evolution of the climatological state, so all terms should be interpreted as climatological time means (and we omit $\langle\rangle$ for the sake of legibility). As in the previous section, we use subscripts c and p to denote variables in the piControl and perturbed (faf-heat) experiments respectively. By $\Phi(\theta)$ we denote the net heat convergence due to *all* heat fluxes in the interior of the ocean, both resolved and parametrised subgridscale. The function Φ depends on diffusivities and other attributes of the model state which affect heat transport, as well as the velocity.

In the piControl experiment,

$$\frac{\partial \theta_c}{\partial t} = Q_c + \Phi_c(\theta_c), \qquad (5)$$

setting the volumetric heat capacity to unity for convenience. The θ field is three-dimensional but Q applies only at the surface.

In faf-heat $\theta = \theta_p$ is affected by the imposed heat flux perturbation F as well as by the atmosphere–ocean heat flux

$Q = Q_p$ simulated by the AOGCM, so

$$\frac{\partial \theta_p}{\partial t} = Q_p + F + \Phi_p(\theta_p), \qquad (6)$$

where Φ_p is a different function from Φ_c because of changed velocities, diffusivities, etc.

The redistributed heat tracer T_R, which we described for method B in Sect. 2.4, is initialised to θ_c and has $Q_p = Q_c + \Delta Q$ as its surface flux, so its evolution equation is

$$\frac{\partial T_R}{\partial t} = Q_p + \Phi_p(T_R). \qquad (7)$$

Since T_R is initialised to θ_c, we write $T_R = \theta_c + \Delta T_R$, i.e. $\Delta T_R = 0$ initially. Let us also split Φ_p into $\Phi_c + \Delta\Phi$. (For example, this splits the advective heat convergence into the part $-\nabla \cdot (T_R \boldsymbol{v}_c)$ due to the piControl velocity field $\boldsymbol{v}_c$ and the part $-\nabla \cdot (T_R \Delta\boldsymbol{v})$ due to the change in the velocity field with respect to the piControl.) These decompositions assume that the heat convergence function depends linearly on the relevant variables of the climate state and acts linearly on the tracers. In that case Eq. (7) becomes

$$\begin{aligned} \frac{\partial T_R}{\partial t} &= Q_c + \Delta Q + \Phi_c(\theta_c) + \Delta\Phi(\theta_c) + \Phi_p(\Delta T_R) \\ &= \Delta Q + \Delta\Phi(\theta_c) + \Phi_p(\Delta T_R) \end{aligned} \qquad (8)$$

if the piControl is a steady state, so that $Q_c + \Phi_c(\theta_c) = 0$ (Eq. 5). T_R is called the "redistributed heat" tracer by Xie and Vallis (2012), because it diagnoses the effect of changes in tracer transport processes (changes in circulation, diffusivities, etc., giving rise to $\Delta\Phi$) on the unperturbed θ_c. If $\Delta\Phi$ vanishes, and assuming $\Delta Q = 0$ as well, $\Delta T_R = 0$ always, meaning that T_R evolves identically to θ_c and thus they remain equal. Changes in ocean heat transport may induce a non-zero ΔQ (Sect. 2.4), which will affect T_R as well.

In order to reveal where the extra heat from the heat flux perturbation is stored in the ocean, we include an "added

Table 3. Ocean model diagnostics of particular interest to FAFMIP analyses (as well as the process-based diagnostics of Table 4).

CMIP short name	Unit	CF standard name
zos	m	sea_surface_height_above_geoid
zostoga	m	global_average_thermosteric_sea_level_change
thetao	°C	sea_water_potential_temperature
*bigthetao	°C	sea_water_conservative_temperature
thetaoga	°C	(volume mean of thetao)
*bigthetaoga	°C	(volume mean of bigthetao)
*opottempmint	$°C\,kg\,m^{-2}$	integral_wrt_depth_of_product_of_sea_water_density_and_potential_temperature
*ocontempmint	$°C\,kg\,m^{-2}$	integral_wrt_depth_of_product_of_sea_water_density_and_conservative_temperature
so	1×10^{-3}	sea_water_salinity
*somint	$1 \times 10^{-3}\,kg\,m^{-2}$	integral_wrt_depth_of_product_of_sea_water_density_and_salinity
msftmyz	$kg\,s^{-1}$	ocean_meridional_overturning_mass_streamfunction
msftyyz	$kg\,s^{-1}$	ocean_y_overturning_mass_streamfunction
hfds	$W\,m^{-2}$	surface_downward_heat_flux_in_sea_water
wfo	$kg\,m^{-2}\,s^{-1}$	water_flux_into_sea_water
*rsdoabsorb	$W\,m^{-2}$	net_rate_of_absorption_of_shortwave_energy_in_ocean_layer
*pathetao	°C	sea_water_additional_potential_temperature
*prthetao	°C	sea_water_redistributed_potential_temperature
*pabigthetao	°C	sea_water_additional_conservative_temperature
*prbigthetao	°C	sea_water_redistributed_conservative_temperature

* Indicates diagnostics which are newly introduced in CMIP6.
The CMIP short names are used by the Climate Model Output Rewriter (CMOR) software and in naming datasets to be submitted to CMIP6. The CF standard names are defined by the CF metadata convention (http://www.cfconventions.org).

heat" tracer T_A in faf-heat. This tracer is initialised to zero (so $\Delta T_A \equiv T_A$) and it has F as its surface flux (we note that heat is added in the global mean, although F is not positive everywhere, as seen in Fig. 2b). Its evolution equation is

$$\frac{\partial T_A}{\partial t} = F + \Phi_p(T_A). \qquad (9)$$

so $T_A = 0$ always if $F = 0$. This tracer is similar to the "passive anomalous temperature" of Banks and Gregory (2006), whose experimental design was different. The added heat tracer is also included in the faf-passiveheat experiment, where its surface source is the same but its evolution is different, because it is subject to the same circulation and subgridscale processes as in the control state, and Φ_c replaces Φ_p in Eq. (9).

Considering Eqs. (6), (7) and (9), we see that

$$\frac{\partial \theta_p}{\partial t} = \frac{\partial T_R}{\partial t} + \frac{\partial T_A}{\partial t}. \qquad (10)$$

Thus we can interpret changes in ocean heat content in faf-heat as the sum of redistribution (including the effect of ΔQ) and addition. In practice, achieving exact equality may not be possible due to non-linearities in the implementation of tracer transport operators.

Careful formulation is required to ensure that Q is applied in the same way to θ and T_R, and some differences may be unavoidable, depending on model formulation. In particular, absorption of solar radiation should occur with the same vertical profile for both (assuming that some of it penetrates the top layer), and the same heat flux should be applied to both of them for evaporation and precipitation (if the sensible heat content of these water fluxes is considered in the model). If the same amount of heat is extracted from both tracers for frazil sea-ice formation, θ may sometimes fall below freezing point, requiring special treatment of the equation of state; on the other hand if θ and T_R are separately kept above freezing, there will be a difference in the heat fluxes implied. Further technical notes can be found at http://www.fafmip.org. It may be useful to check the implementation of T_R in the model with an experiment in which $F = 0$, which should reproduce the piControl experiment.

2.6 Diagnostics

FAFMIP experiments should include standard CMIP6 monthly mean and other diagnostics of atmosphere, ocean and cryosphere, as in the CMIP6 DECK, which is a small set of experiments (including piControl and 1pctCO2) used to evaluate model characteristics of climate and climate change (Eyring et al., 2016). These standard diagnostics provide a large amount of information which will support many kinds of analysis that cannot be anticipated in detail. The standard ocean diagnostics are described in detail for the Ocean Model Intercomparison Project (OMIP) by Griffies et al. (2016) in this issue, and in Table 3 we list a subset of particular importance to FAFMIP, for which they are priority 1 as monthly means. We refer to them here by their CMIP "short names".

Analysis of sea-level change and ocean heat uptake will use diagnostics of sea level, ocean temperature and salinity (`zos`, `zostoga`, `thetao` or `bigthetao`, `thetaoga` or `bigthetaoga`, `opottempmint` or `ocontempmint`, `so` and `somint`, where the choice of alternatives depends on whether the prognostic ocean temperature is potential or conservative). Analyses of the AMOC will use the overturning streamfunction (`msftmyz` or `msftyyz`). The faf-heat and faf-passiveheat experiments should include monthly means of the added heat tracer T_A (`pathetao` or `pabigthetao`), and faf-heat should include monthly means of the redistributed heat tracer T_R (`prthetao` or `prbigthetao`).

Analysis of ocean tracer budgets will use the ocean surface heat and water fluxes requested as standard CMIP monthly diagnostics. Surface fluxes affect only the top layer of the ocean, except for shortwave (solar) radiation, which penetrates more deeply (diagnosed by `rsdoabsorb`). The net surface heat and water fluxes into seawater (`hfds` and `wfo`) are particularly useful, because model-dependent details of implementation, especially regarding sea ice, can make it an intricate or impossible task to compute the net fluxes from other CMIP diagnostics. The net surface flux diagnostics of heat and water are defined somewhat inconsistently by CMIP6 and CF, in that `hfds` should contain Q computed by the model, *not* including the FAFMIP heat flux perturbation, but `wfo` *should* include the FAFMIP water flux perturbation. The FAFMIP steering committee will request each participating group to supply files of the flux perturbations (of momentum, heat and water) as actually applied by them, on the grid of their ocean model, to be made available on the project website for use in inter-comparative analysis.

Inter-comparative analysis of ocean interior change is a priority for FAFMIP, motivating the introduction of the three-dimensional process-based tendency diagnostics for prognostic temperature and salinity (Table 4). These diagnostics are described in detail in Appendix L of Griffies et al. (2016). Different models parametrise interior transports in many ways, so for the purpose of intercomparison it is necessary to aggregate them into broad classes. We distinguish advection by the model velocity field, parametrised eddy advection (mesoscale and submesoscale if treated separately), mesoscale diffusion (by eddies along neutral or isopycnal surfaces), and dianeutral mixing (including diapycnal diffusion, convection and boundary-layer mixing). In addition there is a net tendency diagnostic, whose time-integral over any period should equal the change in the prognostic tracer between the start and end of that period. The difference between the net tendency and the sum of the individual process diagnostics will yield a residual that accounts for any other schemes not separately identified, including the effect of surface fluxes. The tendency diagnostics are expressed as rates of change of heat and salt content in grid cells, i.e. $\partial(mC_p\theta)/\partial t$ and $\partial(mS)/\partial t$, where S is salinity, m is the mass per unit area of the grid cell and C_p the specific heat capacity. In Boussinesq models with fixed cell thicknesses, m is a constant for each grid cell, but otherwise it is variable.

The tendency diagnostics are requested at priority 1 as annual means, and at priority 2 as monthly means for analysis of high-frequency variability, recognising that this implies a substantial amount of storage. Diagnostics of vertical and lateral tracer diffusivity detailed in Appendices M and N of Griffies et al. (2016) are also requested at priority 1 as annual means. The tendency and diffusivity diagnostics should be included in the DECK 1pctCO2 and abrupt4xCO2 experiments, and in the piControl experiment, at least in the portion which is parallel to the FAFMIP experiments as well as in the FAFMIP experiments. These diagnostics will give information which has never previously been available for AOGCMs in general, concerning the roles of the various interior processes in the maintenance of the steady state, unforced variability and the response to climate change.

3 Preliminary results

To test the design, the FAFMIP experiments have been carried out by five groups using existing models from previous phases of CMIP (Table 2). These preliminary experiments did not include the process-based tendency diagnostics described in Sect. 2.6. In order to demonstrate the usefulness of the experiments and stimulate interest in analysis, we present an overview of the results in this section.

3.1 Time dependence of change

Since the imposed FAFMIP surface flux perturbations have no interannual trend or variability, we expect that the ocean will gradually evolve towards a new steady state, as its three-dimensional density and velocity fields adapt to balance the modified surface boundary conditions. The surface fluxes will also evolve as part of this process, because they depend on the surface climate. Time series of global-mean quantities give a useful indication of the approach to the steady state.

3.1.1 Global-mean surface air temperature

The global-mean surface air temperature change ΔT with respect to control reaches a steady state in about 30 years in all the FAFMIP experiments, with time means within $\pm 0.3\,\text{K}$ in most cases (top row of Fig. 5). These are small changes compared with that expected in response to 1pctCO2, in which ΔT after 70 years (at the time of $2 \times CO_2$), referred to as the "transient climate response", has a range of 1.0–2.5 K for CMIP5 AOGCMs. Note that the heat flux perturbation of faf-heat and faf-all does not affect ΔT directly, because T_R is used to supply the SST for the surface climate (Sect. 2.4). Despite the small global mean ΔT, substantial regional changes develop in surface air temperature in all the experiments, and in faf-water all models show a widespread surface cooling. We discuss these points below (Sect. 3.2).

Table 4. New diagnostics for process-based ocean temperature and salinity tendencies, required by FAFMIP and described in detail in Sect. 9 of Griffies et al. (2016).

CMIP short name	CF standard name
opottemptend	tendency_of_sea_water_potential_temperature_expressed_as_heat_content
opottemprmadvect	tendency_of_sea_water_potential_temperature_expressed_as_heat_content_due_to_residual_mean_advection
opottemppadvect	tendency_of_sea_water_potential_temperature_expressed_as_heat_content_due_to_parameterized_eddy_advection
opottemppmdiff	tendency_of_sea_water_potential_temperature_expressed_as_heat_content_due_to_parameterized_mesoscale_diffusion
opottemppsmadvect	tendency_of_sea_water_potential_temperature_expressed_as_heat_content_due_to_parameterized_submesoscale_advection
opottempdiff	tendency_of_sea_water_potential_temperature_expressed_as_heat_content_due_to_parameterized_dianeutral_mixing
ocontemptend	tendency_of_sea_water_conservative_temperature_expressed_as_heat_content
ocontemprmadvect	tendency_of_sea_water_conservative_temperature_expressed_as_heat_content_due_to_residual_mean_advection
ocontemppadvect	tendency_of_sea_water_conservative_temperature_expressed_as_heat_content_due_to_parameterized_eddy_advection
ocontemppmdiff	tendency_of_sea_water_conservative_temperature_expressed_as_heat_content_due_to_parameterized_mesoscale_diffusion
ocontemppsmadvect	tendency_of_sea_water_conservative_temperature_expressed_as_heat_content_due_to_parameterized_submesoscale_advection
ocontempdiff	tendency_of_sea_water_conservative_temperature_expressed_as_heat_content_due_to_parameterized_dianeutral_mixing
osalttend	tendency_of_sea_water_salinity_expressed_as_salt_content
osaltrmadvect	tendency_of_sea_water_salinity_expressed_as_salt_content_due_to_residual_mean_advection
osaltppadvect	tendency_of_sea_water_salinity_expressed_as_salt_content_due_to_parameterized_eddy_advection
osaltpmdiff	tendency_of_sea_water_salinity_expressed_as_salt_content_due_to_parameterized_mesoscale_diffusion
osaltpsmadvect	tendency_of_sea_water_salinity_expressed_as_salt_content_due_to_parameterized_submesoscale_advection
osaltdiff	tendency_of_sea_water_salinity_expressed_as_salt_content_due_to_parameterized_dianeutral_mixing

The units of the temperature tendency diagnostics are $W\,m^{-2}$, and of the salinity tendency diagnostics $kg\,m^{-2}\,s^{-1}$. Either the potential temperature or the conservative temperature diagnostics should be included, depending on which is the prognostic of the model. The effect of advection by the model (resolved) velocity field can be calculated as the difference between the effects of residual mean advection and parametrised eddy advection. The latter should include both mesoscale and submesoscale effects. If these are not distinguished in the model, the diagnostics for parametrised submesoscale advection should be omitted.

3.1.2 Ocean volume-mean temperature

The imposed surface heat flux perturbation in faf-heat is unopposed by increased heat loss to space, because global-mean surface air temperature change is suppressed in method B. Consequently ocean volume-mean temperature rises continuously during faf-heat (second row of Fig. 5). An ocean volume-mean temperature change of 0.1 K is equivalent to an increase in ocean heat content (OHC) of 0.53 YJ, a time-mean heat input of $0.66\,W\,m^{-2}$ averaged over the ocean surface for 70 years, and would produce GMSLR due to thermal expansion of 64 mm (using the CMIP5 model-mean expansion efficiency of heat). By comparison, the change in ocean volume-mean temperature is very small in faf-stress and faf-water. In these experiments, the global OHC is redistributed, as discussed below (Sect. 3.2), with hardly any net change.

3.1.3 Atlantic meridional overturning streamfunction

The time series of change in the AMOC (third row of Fig. 5) are of interest because of its importance to sea-level change in the North Atlantic and regional climate change in Europe. The faf-stress and faf-water experiments show that the perturbations to surface momentum and water fluxes typical of CO_2-induced climate change do not cause significant changes in the AMOC. The grey band in the figure indicates the range $\pm \mathcal{Z}\sqrt{2}\mathcal{S}$ about the control time-mean AMOC, where $\mathcal{S}$ is the interannual standard deviation of the AMOC in the control, $\mathcal{Z} \simeq 1.65$ is the 95th percentile of the normal distribution, and the factor $\sqrt{2}$ is included on the assumption that interannual variation in different experiments is independent. Values of AMOC falling within this band do not differ significantly from the control (10 % two-tailed).

It can be seen from faf-heat that the dominant influence on the AMOC in response to CO_2 is the heat flux perturbation. This has been inferred in some earlier investigations (Rahmstorf and Ganapolski, 1999; Mikolajewicz and Voss, 2000; Gregory et al., 2005), which did not include experiments with heat flux perturbations, although water fluxes were more important in other models (e.g. Dixon et al., 1999). The additional buoyancy flux into the North Atlantic within 80° W–10° E and 30–65° N (the region delimited by a grey box in Fig. 2) due to the heat flux perturbation in faf-heat is more than 40 times larger than that due to the water flux perturbation in faf-water. Heat flux variations have also been found to be the dominant influence on AMOC variability (Delworth et al., 1993; Griffies and Tziperman, 1995; Delworth and Greatbatch, 2000).

As we discuss above (Sect. 2.4), the faf-heat design exaggerates the increase in the surface heat flux in the North Atlantic compared with 1pctCO2. The means of F and ΔQ over the North Atlantic (within the grey box of Fig. 2) are $0.57\,W\,m^{-2}$ and $0.49\,W\,m^{-2}$ (model mean ΔQ, shown for each model in Table 2), so on average the feedback nearly doubles the heat input to this region. Garuba and Klinger (2016) call this effect the "redistribution feedback", and find it is about 70 % of the size of the added heat in the Atlantic. The imposed F and the feedback ΔQ have remarkably similar distributions (Fig. 2b, d). In the rest of the world, the model mean ΔQ is relatively small. Its global mean of $0.07\,W\,m^{-2}$ is much smaller than the global mean F of
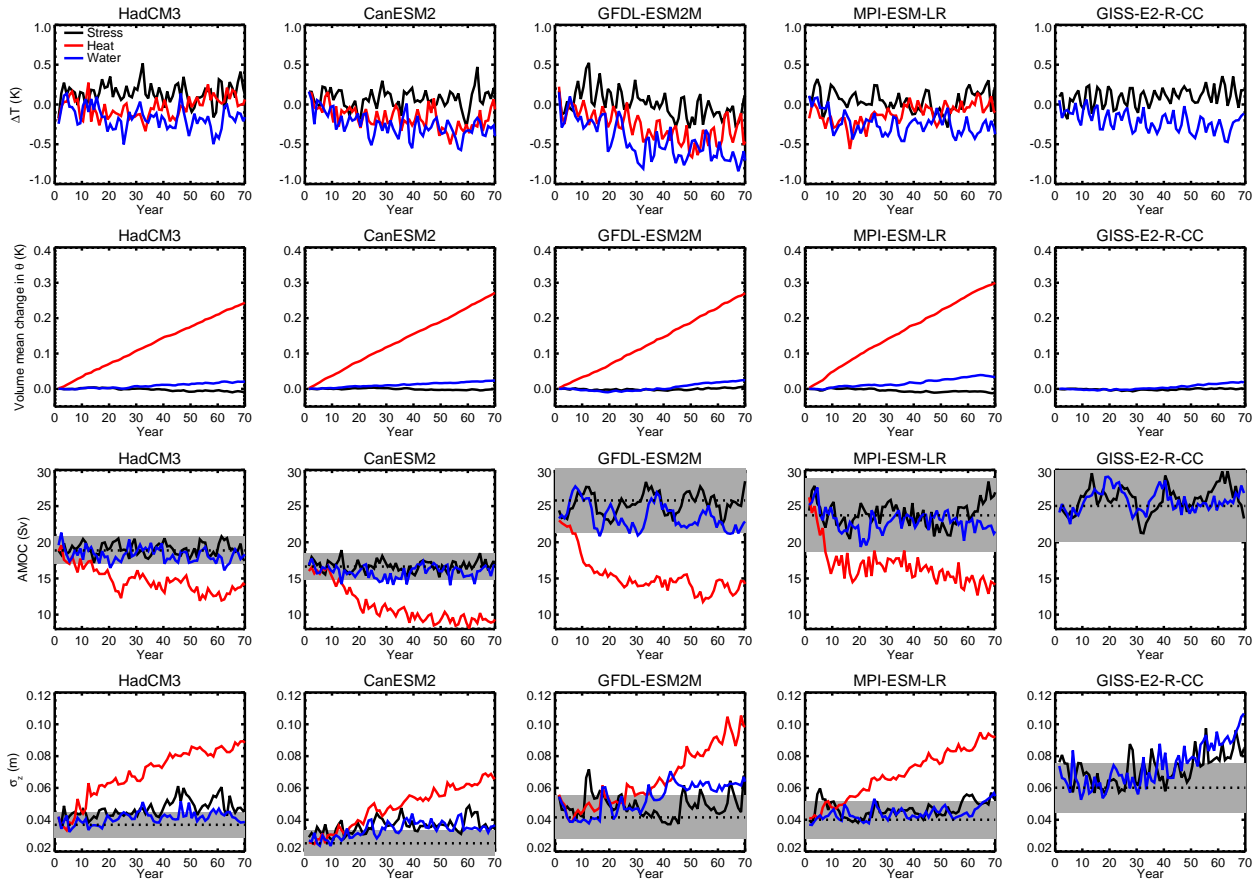
Figure 5. Annual time series in faf-stress, faf-heat and faf-water, according to the key in the first panel. Top row, global-mean surface air temperature change (K) with respect to the control time mean; second row, ocean volume-mean temperature change (K) with respect to the corresponding year of the control; third row, maximum of the Atlantic meridional overturning streamfunction (Sv); bottom row: σ_ζ (m), the spatial standard deviation of $\Delta\zeta$, the dynamic sea-level change relative to the 70-year time mean in the control experiment. For the AMOC and $\Delta\zeta$, the grey band indicates the range of values which do not differ significantly (as defined in the text) from the control time mean, which is indicated by the dotted line.

$1.86\,\mathrm{W\,m^{-2}}$ (shown for individual models in Table 2). Thus it is apparently less important globally in our experiments than in the experiment of Garuba and Klinger (2016), who used an ocean-only model (rather than an AOGCM) with restoring boundary conditions.

Both the magnitude and the time profile of the AMOC weakening in faf-heat are model-dependent (Fig. 5). We presume that the feedback on the heat input also exaggerates the weakening of the AMOC in faf-heat, which is larger than at the time of $2 \times \mathrm{CO_2}$ (using the time mean of years 61–80) in 1pctCO2 experiments with the same AOGCMs (Table 2, ΔAMOC columns). Another reason for a larger response than in 1pctCO2 is that the heat flux perturbation, which is consistent with $2 \times \mathrm{CO_2}$, is applied from the start of the faf-heat experiment.

Although ΔQ always increases the heat flux added to the North Atlantic, the model spread in ΔQ is relatively small (Table 2), so the net addition of heat $F_+ = F + \Delta Q$ in the North Atlantic in faf-heat is quite similar in the four models.

Moreover, although the AMOC weakening is always larger in faf-heat than in 1pctCO2, it correlates between faf-heat and 1pctCO2 across the four AOGCMs, and they are in the same rank order. These points suggest that the faf-heat results may be used to investigate the spread of AMOC weakening in $\mathrm{CO_2}$-forced experiments, despite the amplification.

The area integral of the FAFMIP water flux perturbation field over 50–70° N and 70° W–30° E in the Atlantic is $0.007\,\mathrm{Sv}$. We note that it does not include freshwater input arising from loss of mass by the Greenland ice sheet, because this effect is mostly not included in the CMIP5 AOGCMs from which it was derived. Several studies have evaluated the AMOC response to a freshwater flux of $\sim 0.1\,\mathrm{Sv}$ into the ocean in the vicinity of Greenland. They report a range of results for AMOC weakening, for example by about 2 Sv after several centuries (Vizcaíno et al., 2010), by $1.1 \pm 0.6\,\mathrm{Sv}$ by the end of the 21st century in a comparison of five models (Swingedouw et al., 2015) and by about 5 Sv in fifty years in a comparison of models with 1° and 0.1° resolu-
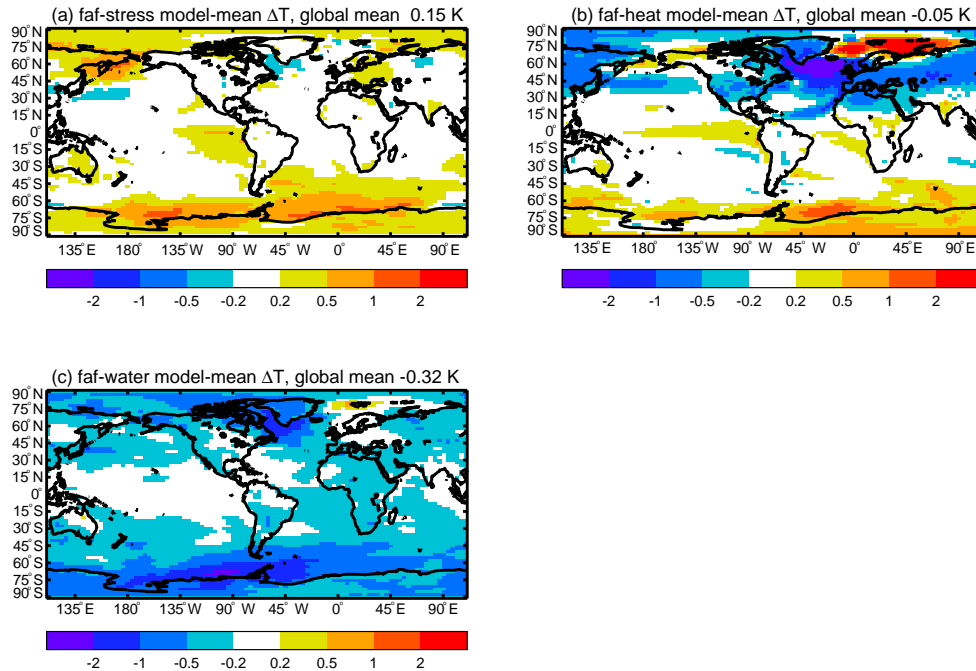
Figure 6. Change in surface air temperature (K) in the time mean of the final decade of the FAFMIP experiments relative to the control. Note that T_R, not θ, is used to supply SST to the atmosphere model in faf-heat, so the change in θ due to the added heat does not affect the surface air temperature (Sect. 2.4, Fig. 3).

tion (Weijer et al., 2012). In the last study, with the eddy-resolving (0.1°) resolution, the AMOC weakening was about 10 Sv when the water flux was applied uniformly over the Atlantic within 50–70° N, following the design of an earlier model intercomparison (Stouffer et al., 2006), in which the AMOC weakening after 100 years showed a large model spread of 0–10 Sv. An addition of 0.1 Sv is a very large perturbation in comparison with the rate of mass loss from the ice sheet during 2002–2011, which was about 200 Gt year^{-1} (Vaughan et al., 2013), equivalent to 0.6 mm year^{-1} of GM-SLR, and 0.006 Sv of freshwater added to the ocean.

3.1.4 Dynamic sea level

To monitor the change in regional sea level, we compute the time series of area-weighted spatial standard deviation $\sigma_\zeta(t)$ of annual mean $\Delta\zeta$ (bottom row of Fig. 5). This quantity is also the spatial standard deviation of $\Delta\eta(\boldsymbol{x}, t)$, since $\Delta\eta$ and $\Delta\zeta$ differ only in their global means. Because of unforced variability within the climate system, local sea level in any given year will differ from its long-term mean, so the control time mean of σ_ζ is not zero. It is model-dependent and in the range 0.02–0.06 m (in agreement with Bilbao et al., 2015, their Fig. 2).

In the perturbed FAFMIP experiments, a forced pattern of $\Delta\zeta$ gradually emerges in addition to and independent of the unforced interannual variability, and σ_ζ thus rises above its control value. In faf-stress and faf-water it levels off within

about 30 years, showing an increase of ~ 0.01 m, and in some experiments it does not differ significantly from the control (comparing with the grey band, calculated as for the AMOC), indicating that sea-level change is not pronounced or widespread, although it may be significant in some regions (Sect. 3.2; for example, the Southern Ocean in faf-stress).

In faf-heat the increase continues for longer and becomes larger; after 70 years it has reached 0.06–0.10 m and has not stabilised. This means that the pattern of $\Delta\zeta$ is increasing in amplitude. In all models σ_ζ in faf-heat becomes significantly different from the control early in the experiment, implying that a statistically detectable geographical pattern of forced change in dynamic sea level has emerged from the background of unforced variability. This idea is related to the global time of emergence, evaluated by Bilbao et al. (2015) using correlation coefficients. The presence of a global pattern of change is detectable before the local change in many regions, and occurs quickly in faf-heat because of the strong forcing applied from the beginning of the experiment.

3.2 Spatial patterns of change

To describe the eventual response to the surface flux perturbations, we consider the state reached by the end of the experiments, as shown by the difference between the time mean of the last decade, years 61–70 and the corresponding decade of the control experiment.
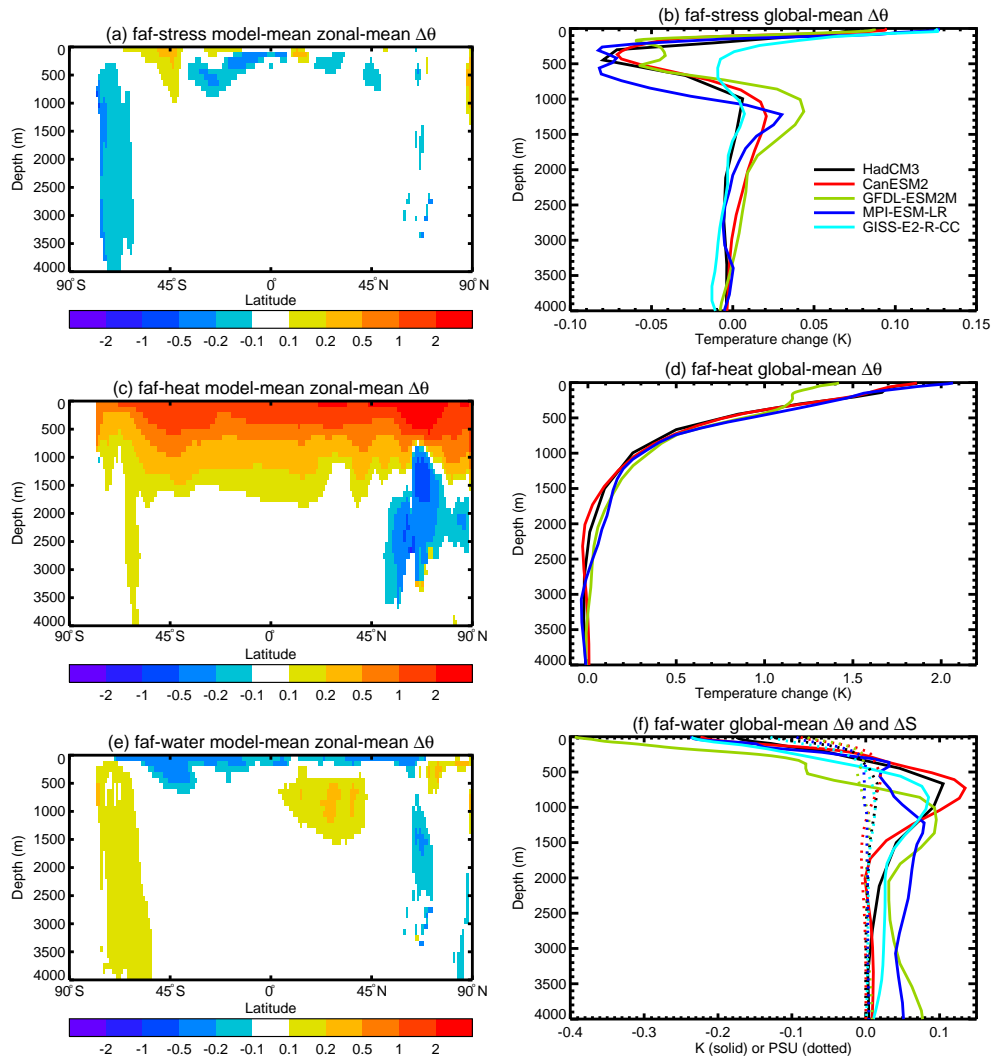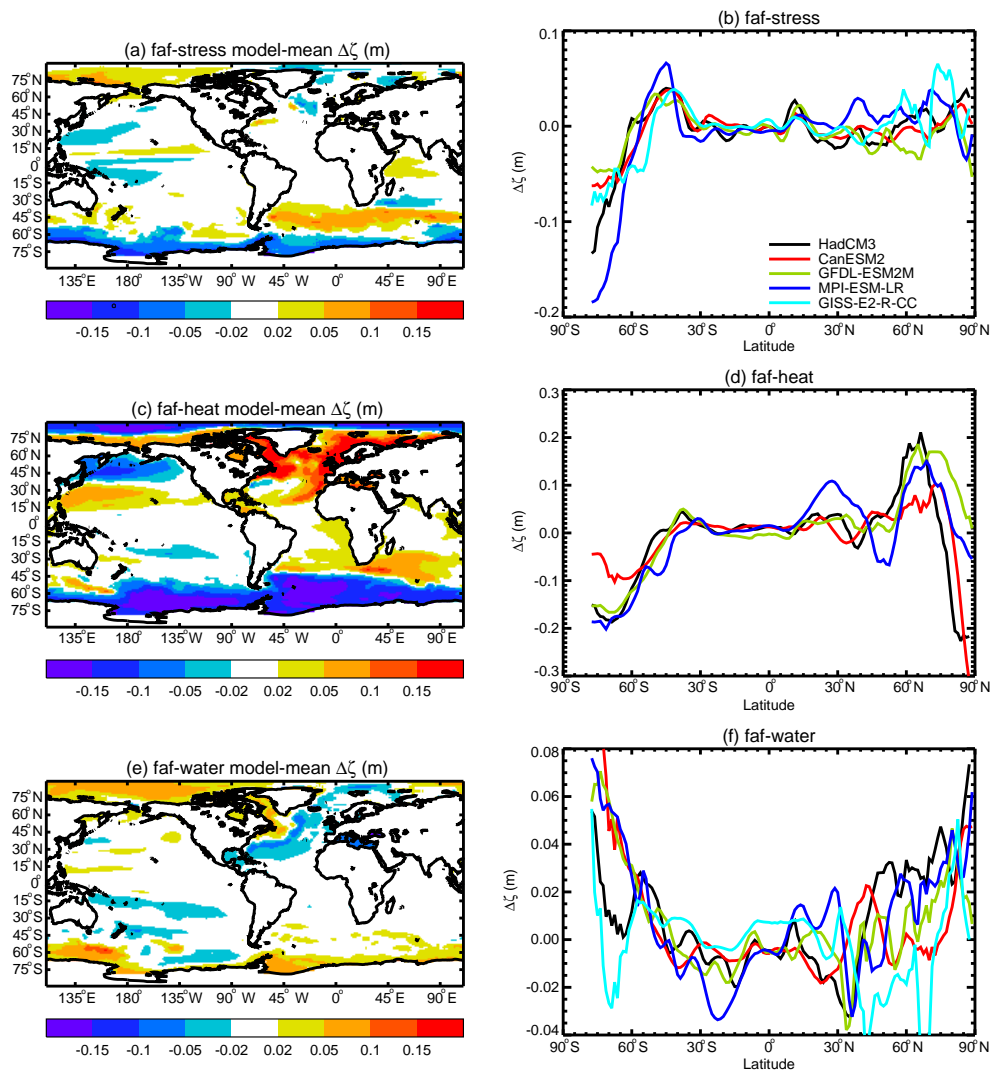
Figure 7. Model-mean change in ocean temperature θ (K) and ocean salinity S (PSU, in **f** only) in the time mean of the final decade of the FAFMIP experiments relative to the control, model-mean zonal-mean cross-sections on the left, global means as a function of depth of individual models on the right. Note that the panels on the right have different scales for the temperature axis.

3.2.1 Surface air temperature

There is warming locally of up to ∼ 1 K in surface air temperature near Antarctica in both faf-stress and faf-heat (Fig. 6a, b). The reduction of heat transport by the AMOC in faf-heat produces a strong cooling of surface air temperature of more than 2 K locally in the North Atlantic and in similar latitudes of Eurasia and North America, as has been found by many previous studies (e.g. Stouffer et al., 2006).

In faf-water, surface air temperature cools over a large fraction of the world (Fig. 6c), by 0.2–0.4 K in the global mean and more than 1 K in some regions. We presume that this is due to the suppression of upward heat transport by a reduction in surface salinity (Fig. 7f). This leads to a downward redistribution of heat from the surface to layers below a few hundred metres (Fig. 7f). A similar tendency to widespread

surface cooling was found by Stammer et al. (2011) in response to the addition of 0.0275 Sv freshwater to the ocean in the vicinity of Greenland. The global integral of the FAFMIP water flux perturbation field is 0.027 Sv and its ocean area average is very small compared with its local values (Fig. 2c). The cooling also occurs in a modified faf-water experiment with HadCM3 and a water flux perturbation field having zero mean (obtained by uniformly subtracting the area average of the standard field), indicating that, at least in this model, the phenomenon is not a response to the global mean of the perturbation flux, but to its geographical pattern through some non-linear mechanism.

Figure 8. Change in dynamic sea level $\Delta\zeta$ (m) in the time mean of the final decade of the FAFMIP experiments relative to the control, model mean on the left, zonal means of individual models on the right. Note that the panels on the right have different scales for the $\Delta\zeta$ axis.

3.2.2 Dynamic sea level

As was intended by the experimental design, the FAFMIP results exhibit the same major features of dynamic sea-level change as found in previous studies for 1pctCO2 and other scenarios (Fig. 8). The heat flux perturbation produces the largest local changes in ζ.

It is interesting to note, by contrast, that over the last couple of decades (the period of continuous satellite sea-level altimetry) the largest regional trends in sea level are caused by momentum flux changes (wind stress) in the Pacific (England et al., 2014; Griffies et al., 2014). The east–west contrast observed in the Pacific is not a pattern predicted in response to CO_2 forcing by AOGCMs (Bilbao et al., 2015; Palanisamy et al., 2015). It may partly be due to unforced multiannual variability associated with the Pacific Decadal Oscillation

and the Southern Oscillation (Merrifield et al., 2012; Zhang and Church, 2012), which is unlikely to be reproduced in AOGCM simulations, even if initialised to an observed state, because predictability is limited (Roberts et al., 2016). Moreover, the observed trends have much greater magnitude than spontaneously generated in AOGCM control experiments. A satisfactory explanation is currently lacking (Clark et al., 2015).

The increased sea-level gradient across the ACC (positive $\Delta\zeta$ to the north and negative to the south) has contributions from both momentum and heat, and is somewhat counteracted by water (Fig. 8; Bouttes and Gregory, 2014; Saenko et al., 2015). Although the momentum and heat flux perturbations are the same in all models, the meridional gradient in $\Delta\zeta$ across the ACC is model-dependent (Fig. 8b, d). Subtracting the global-mean OHC increase from faf-heat reveals
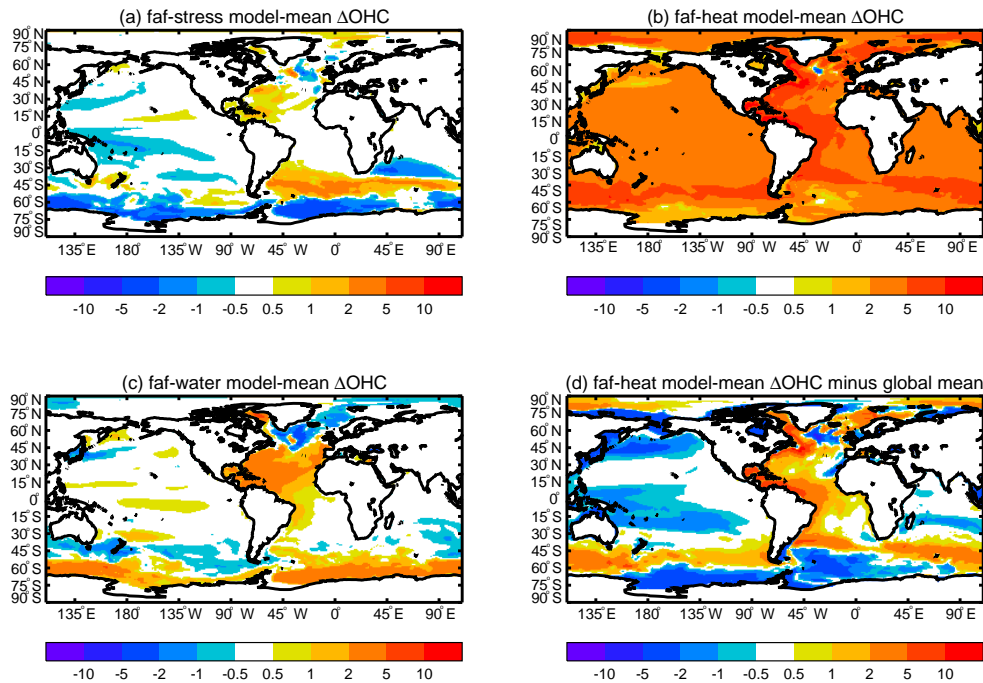
Figure 9. Model-mean change in ocean heat content (GJ m^{-2}, the vertical integral of the change in the ocean temperature θ multiplied by the volumetric heat capacity) in the time mean of the final decade of the FAFMIP experiments relative to the control. Panel **(d)** shows the field of **(b)** with its global mean subtracted.

that the distribution of OHC change is remarkably similar in faf-stress and faf-heat (Fig. 9a, d). From the similarity of $\Delta\zeta$ and changes in local OHC (the vertical integral of θ expressed as heat) in the Southern Ocean in faf-stress (Figs. 8a and 9a), we infer that the effect of the momentum flux perturbation on sea level is predominantly thermosteric rather than halosteric. The increased westerly wind stress strengthens the overturning circulation and redistributes heat northwards to converge around 45°S, where it is pumped downward (Fig. 7a).

The water flux perturbation is positive at high latitudes, and causes positive $\Delta\zeta$ in the Arctic and near Antarctica (Fig. 8e, f). In the Arctic there is reduced OHC and $\Delta\zeta$ is predominantly halosteric, i.e. due to reduced salinity, caused by increased freshwater input (Figs. 2c and 9c). In the Antarctic $\Delta\zeta$ is partly thermosteric, associated with increased OHC (Fig. 9c). It could arise from suppression of upward convective or diffusive heat loss due to reduction of surface salinity and increased stability of the water column, and causes warming to considerable depth in these latitudes (Fig. 7e). Although the AMOC does not change substantially, there is an increase in OHC in much of the Atlantic in faf-water (Figs. 9c and 7e), and a reduction north of ∼ 45° N; this pattern is correlated with (i.e. density-compensated by) the change in salinity content.

The dipole in $\Delta\zeta$ in the North Atlantic (positive to the north of ∼ 40° N, negative to the south) is mainly due to the heat flux perturbation (Fig. 8). It is consistent with a greater

increase in OHC to the north of this latitude in the Atlantic (Fig. 9b, d) and reinforced by changes in salinity (not shown), associated with the weakening of the AMOC in faf-heat (Pardaens et al., 2011; Stammer et al., 2011; Bouttes et al., 2014; Saenko et al., 2015), which reduces northward salinity advection, thus causing an increase in salinity to the south (negative $\Delta\zeta$) and a decrease to the north (positive $\Delta\zeta$). The water flux perturbation contributes to the Atlantic dipole as well (Fig. 8e, f), because it is positive to the north (reducing salinity, raising $\Delta\zeta$) and negative to the south. The momentum perturbation makes no significant contribution to $\Delta\zeta$ in the North Atlantic.

3.3 Addition and redistribution of heat in faf-heat

In faf-heat the added and redistributed heat tracers give us further information about changes in OHC. The greatest surface input of added heat from the heat flux perturbation is to the Southern Ocean (Fig. 2b and 10, grey lines) but the added heat accumulates at lower latitude than the input, due to its wind-driven convergence and subduction centred within 30–45° S (Fig. 10, solid red lines, and Fig. 11e, h). Because of this, the OHC increase near Antarctica is relatively small (Fig. 11d), and $\Delta\zeta$ is negative (Fig. 8c, d), while there is a relatively large addition of heat and positive $\Delta\zeta$ in the southern mid-latitudes, on the north side of the ACC.

The vertical profile of $\Delta\theta$ in faf-heat is dominated by the added heat (Fig. 11a, b). Since the input is at the surface,
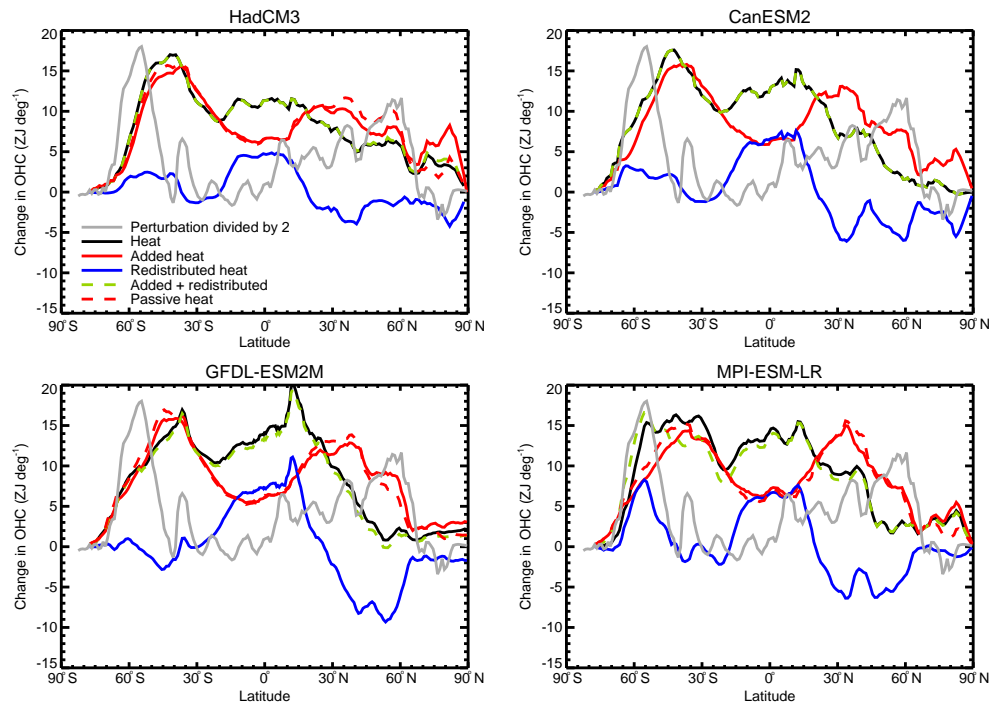
Figure 10. Change in ocean heat content (10^{21} J per degree of latitude) relative to the control in the time mean of the final decade of the faf-heat and faf-passiveheat experiments. The changes in ocean heat content, added heat and redistributed heat are calculated from the integrals over longitude and depth of θ, T_A and T_R respectively, multiplied by volumetric heat capacity. The surface heat flux perturbation F is shown as its integral over longitude and time (for 65 years, to the middle of the final decade), divided by 2 in order to fit on the same axis. The global integrals of F and T_A should be equal.

the concentration of added heat declines with depth in the global mean. There is a minor influence on the vertical profile from redistribution of heat downwards from the surface and upwards from the deep ocean into layers about 500 m deep (Fig. 11c). The small vertical gradient in temperature change between 200 and 500 m in GFDL-ESM2M is due to redistribution; it relates to a cooling in the shallow tropics and resembles the response of the same model to volcanic forcing (Stenchikov et al., 2009, their Fig. 3) with the opposite sign. Heat is redistributed from the mid-latitude gyres, around 30° in both hemispheres, towards the Equator (Fig. 10, blue lines, and Fig. 11f, i). Comparison of Figs. 11f and 9d is useful for appreciating the relative importance of addition and redistribution of heat in setting the geographical pattern of OHC change.

Marked changes occur in the North Atlantic associated with the AMOC, although they do not dominate the global picture because the Atlantic has a relatively small area. Deep water formation conveys added heat to the deep North Atlantic around 60° N (Fig. 11h). The weakening of the AMOC tends to reduce northward and downward heat transport, causing redistributive cooling throughout the North Atlantic (Fig. 11f, i), except in a narrow band along the east coast of North America, where the weakened northward transport in the boundary current reduces the divergence

of heat, increases OHC and enhances $\Delta\zeta$ (Yin et al., 2009; Bouttes et al., 2014). In the deep North Atlantic, negative redistribution outweighs positive addition of heat, and a net cooling results (Fig. 11g).

As intended by construction (Sect. 2.4), the sum of added and redistributed heat is very similar or identical to the change in OHC (Fig. 10, compare black and green lines). The volume integral of the redistributed heat is not zero because it is affected by ΔQ (Table 2). Nonetheless it is small (0.03–0.08 YJ) compared with the added heat (1.32–1.35 YJ), whose variation across models arises from different land–sea boundaries, ocean area and regridding methods. The latitudinal distribution of added heat is very similar in faf-heat and faf-passiveheat (Fig. 10, compare red solid and dashed lines), especially in the Southern Hemisphere. This indicates that the influence of change in transport on the added heat is of second order, as expected. South of 30° S, changes in OHC and added heat are fairly similar in the zonal integral (Fig. 10, compare solid red and black lines), i.e. redistribution is relatively small, and heat uptake is largely passive.
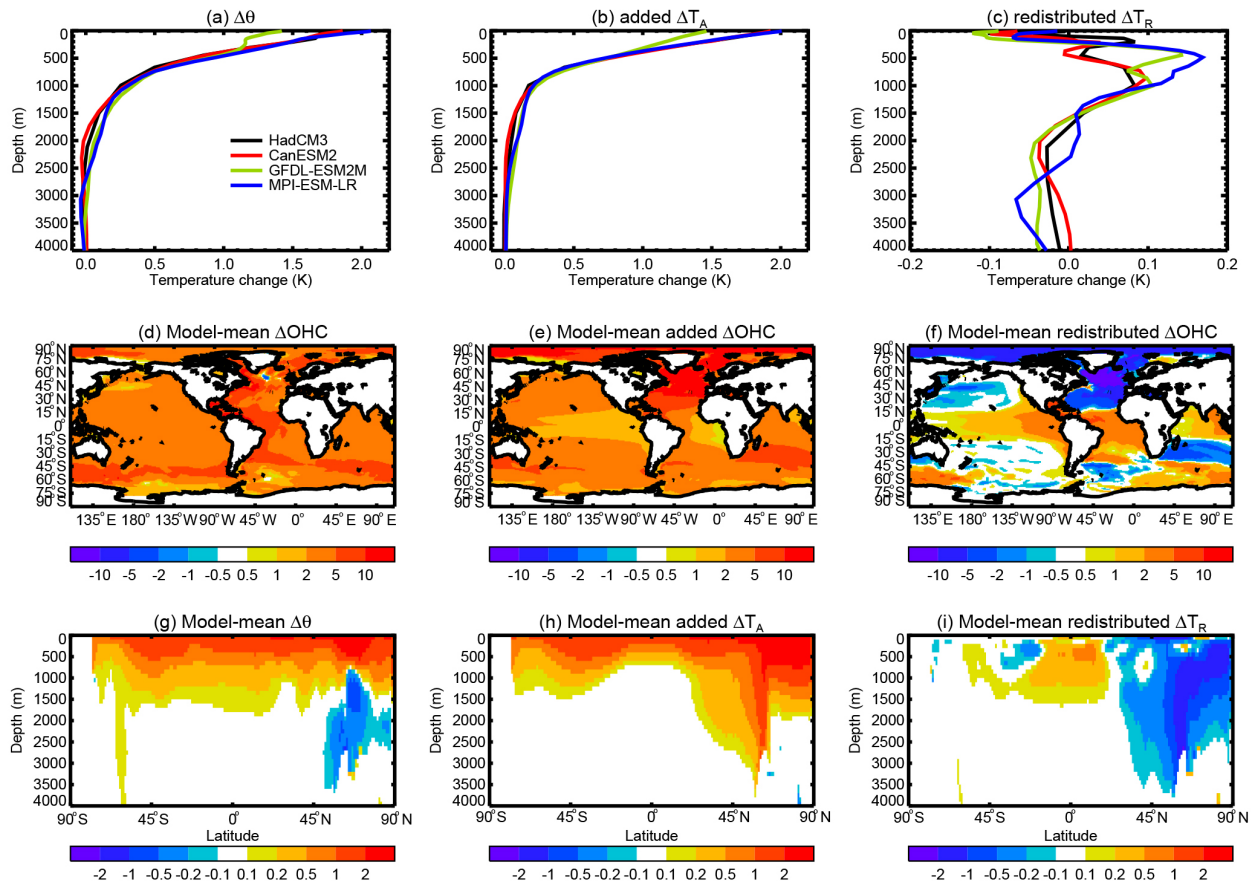
Figure 11. Change in ocean temperature θ (left) and tracers of added heat (centre) and redistributed heat (right) in the final decade of the faf-heat experiment, (top) global-mean change in tracer (K) as a function of depth, with different scales for the temperature axis, (middle) model-mean change in heat content (GJ m^{-2}, the vertical integral of the change in tracer multiplied by volumetric heat capacity), (bottom) model-mean zonal-mean cross-sections of the change in tracer (K). Panels (**a, d, g**) are the same as Figs. 7d, c and 9b respectively, and are repeated here for ease of comparison.

4   Summary and plans

The purpose of the Flux-Anomaly-Forced Model Intercomparison Project is to analyse the simulated response of the ocean to changes in surface fluxes resulting from CO_2 forcing in AOGCMs. The specific interests which motivated the proposal of FAFMIP are

 – The magnitude of ocean heat uptake in response to climate change, which determines global-mean sea-level rise due to thermal expansion and influences the transient climate response.

 – The geographical patterns of sea-level change due to ocean density and circulation change simulated by the models.

 – The weakening of the Atlantic meridional overturning circulation, which affects regional sea-level rise and climate change.

 – The ocean's role in determining the patterns of sea-surface temperature change, which influences climate sensitivity to CO_2.

 – Subsurface warming of the ocean near to the Greenland and Antarctic ice sheets, where it might enhance basal melting of ice shelves and hence sea-level rise through the dynamical response of the ice-sheets.

These topics are all aspects of the Earth system response to forcing, and they are of particular relevance to the WCRP Grand Challenges on regional sea-level rise, melting ice, and climate sensitivity. The motivation for FAFMIP is to find ways of reducing the uncertainty in projections in policy-relevant scenarios, by applying observational constraints and improved physical understanding to refine the models.

In the FAFMIP tier-1 experiments faf-stress, faf-heat and faf-water, prescribed perturbations are applied to the ocean surface in the fluxes of momentum, heat and freshwater respectively. The flux perturbations have a seasonal cycle but no interannual variation, and are obtained from a model mean

of changes simulated in CMIP5 AOGCM experiments at year 70 in 1pctCO2 experiments (with CO_2 increasing at 1 % year^{-1}). They are thus typical of simulated CO_2-forced climate change in magnitude and geographical pattern. The intention of applying the same surface flux perturbations in all AOGCMs in FAFMIP is to reveal the dependence of the response on the ocean model. The FAFMIP tier-1 experiments amount to 210 years of integration, which is a modest requirement compared with many CMIP6 subprojects. There are two tier-2 experiments of 70 years each, one of which can be achieved by adding a diagnostic to the control experiment, thereby avoiding the need for a separate integration. We have carried out preliminary tier-1 experiments with pre-CMIP6 AOGCMs to test and demonstrate the experimental design. Our models exhibit diversity in the pattern and magnitude of simulated changes, with some common qualitative features.

We find that momentum and water flux perturbation do not affect the AMOC significantly, but the AMOC weakens in faf-heat, by 6–12 Sv depending on the model, in response to the heat added to the North Atlantic. The AMOC weakening is reinforced by a feedback on the surface heat flux whereby, as the AMOC declines, the SST in the North Atlantic tends to cool, so the heat flux from the atmosphere to the ocean increases (Rahmstorf and Willebrand, 1995; Marotzke, 1996). This effectively doubles the heat flux perturbation in that region (although it is a small effect in the global mean). Consequently the AMOC weakening in faf-heat is larger than the expected response for 1pctCO2. However, the net extra heat input to the North Atlantic, including the feedback, is similar in all the models, indicating that the model spread in AMOC weakening in faf-heat is mainly due to differences in ocean model response, rather than to a spread in the buoyancy forcing.

Despite its exaggerated magnitude, this coupled feedback is a physical effect which must also occur in the CMIP5 1pctCO2 experiments from which the heat flux perturbation was derived (Winton et al., 2013), and presumably in general in climate change simulated by AOGCMs. Our results therefore strongly suggest that it is an important effect on the weakening of the AMOC in response to CO_2 forcing, and may not have been sufficiently appreciated. Stammer et al. (2011) found a similar large positive feedback from increased heat input on the weakening of the AMOC in response to addition of freshwater around Greenland. We note that the positive feedback on AMOC weakening is a distinct effect from the negative feedback on AMOC weakening in which the cooling in the North Atlantic promotes convection and deep water formation and tends to strengthen the circulation (e.g. Marotzke, 1996). The negative feedback is an oceanic phenomenon, not a coupled one.

Global-mean surface air temperature cools over a large fraction of the world in faf-water, by 0.3 K in the global model mean. The global-mean input by the water flux perturbation is very small compared with its local values (its ocean area mean is 7.2×10^{-8} kg m^{-2} s^{-1}, 2 orders of mag-

nitude smaller than its spatial standard deviation of 5.4×10^{-6} kg m^{-2} s^{-1}), so the phenomenon is probably a response to its geographical pattern. Global-mean surface temperature change is small in faf-stress and faf-heat (note that the heat added to the ocean in faf-heat is prevented from directly affecting the surface air temperature), but there is substantial warming near to Antarctica and in the Arctic, and strong cooling in the North Atlantic and northern mid-latitude land areas in faf-heat associated with the AMOC weakening. Heat is added in faf-heat mainly at high latitude, and is transported equatorward and downward in a model-dependent way. This implies a spread in ocean heat uptake efficiency and global-mean sea-level rise due to thermal expansion.

As in many previous studies, the main geographical features of dynamic sea-level change are an increase in the gradient across the ACC (small sea-level rise to the south, large to the north), a dipole in the North Atlantic (small sea-level rise in the subtropical gyre, large sea-level rise to the north), and enhanced sea-level rise in the Arctic. We find that the Southern Ocean feature is caused in roughly equal measure by momentum and heat flux perturbations, and somewhat counteracted by the water flux perturbation. In the Southern Ocean, where there is the greatest increase in ocean heat content in faf-heat, heat uptake is largely passive, while in faf-stress there is wind-driven redistribution of heat from high to low latitude. The Arctic feature is mainly due to the water flux perturbation. The North Atlantic feature results from the heat and water flux perturbations, which both give a meridional contrast in buoyancy flux (greater to the north, causing more sea-level rise). In faf-heat this effect is opposed by reduced heat transport due to the weakening of the AMOC, which redistributes heat from high to low northern latitude. Redistribution is also responsible for strongly enhanced sea-level rise along the Atlantic coast of North America in faf-heat.

The results from the pre-CMIP6 trial experiments show that there will be many qualitative and quantitative features to be analysed in CMIP6. The CMIP6 FAFMIP experiments and the piControl and idealised CO_2 experiments with FAFMIP models will contain diagnostics for rates of change of temperature and salinity due to separate ocean interior transport processes (advection, diffusion, etc.). Such diagnostics have been available in only a few models previously, and were not included in the preliminary experiments that we have carried out for this paper. They will yield a great deal of new information. In the piControl the diagnostics will enable us to study the balance of ocean processes in the mean state and unforced variability of the coupled atmosphere–ocean system. In the FAFMIP experiments and the idealised CO_2 climate-change experiments they will allow us to identify the mechanistic explanations both for the common features of the model responses to surface flux forcing and for the differences among models.

The FAFMIP steering committee will promote the analysis of the experiments, bearing in mind the scientific ques-

tions which motivated the project. Comparison of the results from different AOGCMs will aim to identify the causes of the spread in their simulated climate change, in terms of model formulation and emergent behaviour. We envisage that in the light of further analysis we may devise additional tier-2 experiments, for instance to study the effect of surface heat flux feedbacks. It may also be useful to carry out ensemble experiments to quantify the influence of unforced variability, although the major features of the forced response are expected to be robust in view of the large size of the perturbations. Using the faf-all experiment, the effect of combining the flux perturbations will be studied.

The application of common surface flux perturbations is a technique which has not been widely used up to now as a means to study ocean climate change simulated by AOGCMs in response to CO_2 forcing. We therefore hope that the FAFMIP experiments will offer new insight into the reasons for model spread in the ocean response, without the confounding influence of diversity in atmospheric response. Where the patterns of ocean climate change differ among the models in FAFMIP experiments, we expect that these differences will correspond to those which the models exhibit in the AOGCM scenario-forced projections. On the other hand, when the ocean models agree in FAFMIP experiments, it will give us greater confidence in the results, and we will be able to infer that the atmosphere models are the source of uncertainty in projections of ocean climate change.

5   Data availability

The model output from the DECK and CMIP6 historical simulations described in this paper will be distributed through the Earth System Grid Federation (ESGF) with digital object identifiers (DOIs) assigned. As in CMIP5, the model output will be freely accessible through data portals after registration. In order to document CMIP6's scientific impact and enable ongoing support of CMIP, users are obligated to acknowledge CMIP6, the participating modelling groups, and the ESGF centres (see details on the CMIP Panel website at http://www.wcrp-climate.org/index.php/wgcm-cmip/about-cmip).

Further information about the infrastructure supporting CMIP6, the metadata describing the model output, and the terms governing its use are provided by the WGCM Infrastructure Panel (WIP) in their invited contribution to this Special Issue (Balaji et al., 2016). Along with the data itself, the provenance of the data will be recorded, and DOIs will be assigned to collections of output so that they can be appropriately cited. This information will be made readily available so that published research results can be verified and credit can be given to the modelling groups providing the data. The WIP is coordinating and encouraging the development of the infrastructure needed to archive and deliver this information. In order to run the experiments, datasets for natural and anthropogenic forcings are required. These forcing datasets are described in separate invited contributions to this Special Issue. The forcing datasets will be made available through the ESGF with version control and DOIs assigned.

Edited by: R. Marsh
Reviewed by: two anonymous referees

References

Balaji, V., Taylor, K., Cinquini, L., DeLuca, C., Denvil, S., Elkington, M., Guglielmo, F., Guilyardi, E., Juckes, M., Kharin, S., Lautenschlager, M., Lawrence, B., and Williams, D.: Global Data Infrastructure Requirements for CMIP6, Geosci. Model Dev. Discuss., in preparation, 2016.

Banks, H. T. and Gregory, J. M.: Mechanisms of ocean heat uptake in a coupled climate model and the implications for tracer based predictions of ocean heat uptake, Geophys. Res. Lett., 33, L07608, doi:10.1029/2005GL025352, 2006.

Banks, H. T., Stark, S., and Keen, A. B.: The adjustment of the coupled climate model HadGEM1 towards equilibrium and the impact on global climate, J. Climate, 20, 5815–5826, doi:10.1175/2007JCLI1688.1, 2007.

Bilbao, R. A. F., Gregory, J. M., and Bouttes, N.: Analysis of the regional pattern of sea level change due to ocean dynamics and density changes for 1993–2099 in observations and CMIP5 AOGCMs, Clim. Dynam., 45, 2647–2666, doi:10.1007/s00382-015-2499-z, 2015.

Böning, C. W., Dispert, A., Visbeck, M., Rintoul, S. R., and Schwarzkopf, F. U.: The response of the Antarctic Circumpolar Current to recent climate change, Nat. Geosci., 1, 864–869, doi:10.1038/ngeo362, 2008.

Bouttes, N. and Gregory, J. M.: Attribution of the spatial pattern of CO_2-forced sea level change to ocean surface flux changes, Environ. Res. Lett., 9, 034004, doi:10.1088/1748-9326/9/3/034004, 2014.

Bouttes, N., Gregory, J. M., Kuhlbrodt, T., and Suzuki, T.: The effect of windstress change on future sea level change in the Southern Ocean, Geophys. Res. Lett., 39, L23602, doi:10.1029/2012GL054207, 2012.

Bouttes, N., Gregory, J. M., Kuhlbrodt, T., and Smith, R. S.: The drivers of projected North Atlantic sea level change, Clim. Dynam., 43, 1531–1544, doi:10.1007/s00382-013-1973-8, 2014.

Church, J. A., Gregory, J. M., Huybrechts, P., Kuhn, M., Lambeck, K., Nhuan, M. T., Qin, D., and Woodworth, P. L.: Changes in sea level, in: Climate change 2001: The scientific basis. Contribution of Working Group I to the Third Assessment Report of the Intergovernmental Panel on Climate Change, edited by: Houghton, J. T., Ding, Y., Griggs, D. J., Noguer, M., van der Linden, P., Dai, X., Maskell, K., and Johnson, C. I., 639–693, Cambridge University Press, 2001.

Church, J. A., Clark, P. U., Cazenave, A., Gregory, J. M., Jevrejeva, S., Levermann, A., Merrifield, M. A., Milne, G. A., Nerem, R. S., Nunn, P. D., Payne, A. J., Pfeffer, W. T., Stammer, D., and Unnikrishnan, A. S.: Sea Level Change, in: Climate Change 2013: The Physical Science Basis. Contribution of Working Group I to the Fifth Assessment Report of the Intergovernmental Panel on Climate Change, edited by: Stocker, T. F., Qin, D., Plattner, G.-K., Tignor, M., Allen, S. K., Boschung, J., Nauels, A., Xia, Y., Bex, V., and Midgley, P. M., Cambridge University Press, doi:10.1017/CBO9781107415324.026, 2013.

Clark, P. U., Church, J. A., Gregory, J. M., and Payne, A. J.: Recent progress in understanding and projecting regional and global mean sea-level change, Current Climate Change Reports, 1, 224–246, doi:10.1007/s40641-015-0024-4, 2015.

Collins, M., Knutti, R., Arblaster, J. M., Dufresne, J., Fichefet, T., Friedlingstein, P., Gao, X., Gutowski, W. J., Johns, T., Krinner, G., Shongwe, M., Tebaldi, C., Weaver, A. J., and Wehner, M.: Long-term Climate Change: Projections, Commitments and Irreversibility, in: Climate Change 2013: The Physical Science Basis. Contribution of Working Group I to the Fifth Assessment Report of the Intergovernmental Panel on Climate Change, edited by: Stocker, T. F., Qin, D., Plattner, G.-K., Tignor, M., Allen, S. K., Boschung, J., Nauels, A., Xia, Y., Bex, V., and Midgley, P. M., 1029–1136, Cambridge University Press, doi:10.1017/CBO9781107415324.024, 2013.

Cubasch, U., Meehl, G. A., Boer, G. J., Stouffer, R. J., Dix, M., Noda, A., Senior, C. A., Raper, S. C. B., and Yap, K. S.: Projections of future climate change, in: Climate change 2001: The scientific basis. Contribution of Working Group I to the Third Assessment Report of the Intergovernmental Panel on Climate Change, edited by: Houghton, J. T., Ding, Y., Griggs, D. J., Noguer, M., van der Linden, P., Dai, X., Maskell, K., and Johnson, C. I., 525–582, Cambridge University Press, 2001.

Danabasoglu, G.: A comparison of global ocean general circulation model solutions obtained with synchronous and accelerated integration methods, Ocean Model., 7, 323–341, doi:10.1016/j.ocemod.2003.10.001, 2004.

Delworth, T. L. and Greatbatch, R. J.: Multidecadal thermohaline circulation variability driven by atmospheric flux forcing, J. Climate, 13, 1481–1495, 2000.

Delworth, T. L., Manabe, S., and Stouffer, R. J.: Interdecadal variations of the thermohaline circulation in a coupled ocean-atmosphere model, J. Climate, 6, 1993–2011, 1993.

Dixon, K. W., Delworth, T. L., Spelman, M. J., and Stouffer, R. J.: The influence of transient surface fluxes on North Atlantic overturning in a coupled GCM climate change experiment, Geophys. Res. Lett., 26, 2749–2752, 1999.

Downes, S. M. and Hogg, A. M.: Southern Ocean circulation and eddy compensation in CMIP5 models, J. Climate, 26, 7198–7220, doi:10.1175/JCLI-D-12-00504.1, 2013.

Dunne, J. P., John, J. G., Hallberg, R. W., Griffies, S. M., Shevliakova, E. N., Stouffer, R. J., Krasting, J. P., Sentman, L. A., Milly, P. C. D., Malyshev, S. L., Adcroft, A. J., Cooke, W., Dunne, K. A., Harrison, M. J., Levy, H., Samuels, B. L., Spelman, M., Winton, M., Wittenberg, A. T., Phillips, P. J., and Zadeh, N.: GFDL's ESM2 global coupled climate-carbon Earth System Models Part I: Physical formulation and baseline simulation characteristics, J. Climate, 25, 6646–6665, doi:10.1175/JCLI-D-11-00560.1, 2012.

England, M. H., McGregor, S., Spence, P., Meehl, G. A., Timmermann, A., Cai, W., Gupta, A. S., McPhaden, M. J., Purich, A., and Santoso, A.: Recent intensification of wind-driven circulation in the Pacific and the ongoing warming hiatus, Nature Climate Change, 4, 222–227, doi:10.1038/nclimate2106, 2014.

Exarchou, E., Kuhlbrodt, T., Gregory, J. M., and Smith, R. S.: Ocean heat uptake processes: a model intercomparison, J. Climate, 28, 887–908, doi:10.1175/jcli-d-14-00235.1, 2015.

Eyring, V., Bony, S., Meehl, G. A., Senior, C. A., Stevens, B., Stouffer, R. J., and Taylor, K. E.: Overview of the Coupled Model Intercomparison Project Phase 6 (CMIP6) experimental design and organization, Geosci. Model Dev., 9, 1937–1958, doi:10.5194/gmd-9-1937-2016, 2016.

Farneti, R., Delworth, T. L., Rosati, A. J., Griffies, S. M., and Zeng, F.: The role of mesoscale eddies in the rectification of the Southern Ocean response to climate change, J. Phys. Oceanogr., 40, 1539–1557, 2010.

Farneti, R., Downes, S. M., Griffies, S. M., Marsland, S. J., Behrens, E., Bentsen, M., Bi, D., Biastoch, A., Böning, C. W., Bozec, A., Canuto, V. M., Chassignet, E., Danabasoglu, G., Danilov, S., Diansky, N., Drange, H., Fogli, P. G., Gusev, A., Hallberg, R. W., Howard, A., Ilicak, M., Jung, T., Kelley, M., Large, W. G., Leboissetier, A., Long, M., Lu, J., Masinam, S., Mishra, A., Navarra, A., Nurser, A. J. G., Patara, L., Samuels, B. L., Sidorenko, D., Tsujino, H., Uotila, P., Wang, Q., and Yeager, S. G.: An assessment of Antarctic Circumpolar Current and Southern Ocean meridional overturning circulation during 1958–2007 in a suite of interannual CORE-II simulations, Ocean Model., 94, 84–120, doi:10.1016/j.ocemod.2015.07.009, 2015.

Frankcombe, L. M., Spence, P., Hogg, A. M., England, M. H., and Griffies, S. M.: Sea level changes forced by Southern Ocean winds, Geophys. Res. Lett., 40, 5710–5715, doi:10.1002/2013GL058104, 2013.

Garuba, O. and Klinger, B.: Ocean heat uptake and interbasin transport of passive and redistributive surface heating, J. Climate, 29, 7507–7527, doi:10.1175/JCLI-D-16-0138.1, 2016.

Gent, P. R. and McWilliams, J. C.: Isopycnal mixing in ocean circulation models, J. Phys. Oceanogr., 20, 150–155, doi:10.1175/1520-0485(1990)020<0150:IMIOCM>2.0.CO;2, 1990.

Giorgetta, M. A., Jungclaus, J., Reick, C. H., Legutke, S., Bader, J., Boettinger, M., Brovkin, V., Crueger, T., Esch, M., Fieg, K., Glushak, K., Gayler, V., Haak, H., Hollweg, H.-D., Ilyina, T., Kinne, S., Kornblueh, L., Matei, D., Mauritsen, T., Mikolajewicz, U., Mueller, W., Notz, D., Pithan, F., Raddatz, T., Rast, S., Redler, R., Roeckner, E., Schmidt, H., Schnur, R., Segschneider, J., Six, K. D., Stockhause, M., Timmreck, C., Wegner, J.,

Widmann, H., Wieners, K.-H., Claussen, M., Marotzke, J., and Stevens, B.: Climate and carbon cycle changes from 1850 to 2100 in MPI-ESM simulations for the Coupled Model Intercomparison Project phase 5, J. Adv. Model Earth Syst., 5, 572–597, doi:10.1002/jame.20038, 2013.

Gordon, C., Cooper, C., Senior, C. A., Banks, H., Gregory, J. M., Johns, T. C., Mitchell, J. F. B., and Wood, R. A.: The Simulation of SST, sea ice extents and ocean heat transports in a version of the Hadley Centre coupled model without flux adjustments, Clim. Dynam., 16, 147–168, doi:10.1007/s003820050010, 2000.

Gregory, J. M.: Vertical heat transports in the ocean and their effect on time-dependent climate change, Clim. Dynam., 16, 501–515, doi:10.1007/s003820000059, 2000.

Gregory, J. M. and Mitchell, J. F. B.: The climate response to CO_2 of the Hadley Centre coupled AOGCM with and without flux adjustment, Geophys. Res. Lett., 24, 1943–1946, doi:10.1029/97GL01930, 1997.

Gregory, J. M., Church, J. A., Boer, G. J., Dixon, K. W., Flato, G. M., Jackett, D. R., Lowe, J. A., O'Farrell, S. P., Roeckner, E., Russell, G. L., Stouffer, R. J., and Winton, M.: Comparison of results from several AOGCMs for global and regional sea-level change 1900–2100, Clim. Dynam., 18, 225–240, doi:10.1007/s003820100180, 2001.

Gregory, J. M., Dixon, K. W., Stouffer, R. J., Weaver, A. J., Driesschaert, E., Eby, M., Fichefet, T., Hasumi, H., Hu, A., Jungclaus, J. H., Kamenkovich, I. V., Levermann, A., Montoya, M., Murakami, S., Nawrath, S., Oka, A., Sokolov, A. P., and Thorpe, R. B.: A model intercomparison of changes in the Atlantic thermohaline circulation in response to increasing atmospheric CO_2 concentration, Geophys. Res. Lett., 32, L12703, doi:10.1029/2005GL023209, 2005.

Griffies, S. and Tziperman, E.: A linear thermohaline oscillator driven by stochastic atmospheric forcing, J. Climate, 8, 2440–2453, 1995.

Griffies, S. M.: The Gent-McWilliams skew-flux, J. Phys. Oceanogr., 28, 831–841, 1998.

Griffies, S. M. and Greatbatch, R. J.: Physical processes that impact the evolution of global mean sea level in ocean climate models, Ocean Model., 51, 37–72, doi:10.1016/j.ocemod.2012.04.003, 2012.

Griffies, S. M., Yin, J., Durack, P. J., Goddard, P., Bates, S. C., Behrens, E., Bentsen, M., Bi, D., Biastoch, A., Boening, C. W., Bozec, A., Chassignet, E., Danabasoglu, G., Danilov, S., Domingues, C. M., Drange, H., Farneti, R., Fernandez, E., Greatbatch, R. J., Holland, D. M., Ilicak, M., Large, W. G., Lorbacher, K., Lu, J., Marsland, S. J., Mishra, A., Nurser, A. J. G., Salas y Melia, D., Palter, J. B., Samuels, B. L., Schroeter, J., Schwarzkopf, F. U., Sidorenko, D., Treguier, A. M., Tseng, Y.-H., Tsujino, H., Uotila, P., Valcke, S., Voldoire, A., Wang, Q., Winton, M., and Zhang, X.: An assessment of global and regional sea level for years 1993–2007 in a suite of interannual CORE-II simulations, Ocean Model., 78, 35–89, doi:10.1016/j.ocemod.2014.03.004, 2014.

Griffies, S. M., Winton, M., Anderson, W. G., Benson, R., Delworth, T. L., Dufour, C., Dunne, J. P., Goddard, P., Morrison, A. K., Rosati, A., Wittenberg, A. T., and Yin, J.: Impacts on ocean heat from transient mesoscale eddies in a hierarchy of climate models, J. Climate, 28, 952–977, doi:10.1175/JCLI-D-14-00353.1, 2015.

Griffies, S. M., Danabasoglu, G., Durack, P. J., Adcroft, A. J., Balaji, V., Böning, C. W., Chassignet, E. P., Curchitser, E., Deshayes, J., Drange, H., Fox-Kemper, B., Gleckler, P. J., Gregory, J. M., Haak, H., Hallberg, R. W., Heimbach, P., Hewitt, H. T., Holland, D. M., Ilyina, T., Jungclaus, J. H., Komuro, Y., Krasting, J. P., Large, W. G., Marsland, S. J., Masina, S., McDougall, T. J., Nurser, A. J. G., Orr, J. C., Pirani, A., Qiao, F., Stouffer, R. J., Taylor, K. E., Treguier, A. M., Tsujino, H., Uotila, P., Valdivieso, M., Wang, Q., Winton, M., and Yeager, S. G.: OMIP contribution to CMIP6: experimental and diagnostic protocol for the physical component of the Ocean Model Intercomparison Project, Geosci. Model Dev., 9, 3231–3296, doi:10.5194/gmd-9-3231-2016, 2016.

Hallberg, R., Adcroft, A., Dunne, J. P., Krasting, J. P., and Stouffer, R. J.: Sensitivity of twenty-first-century global-mean steric sea level rise to ocean model formulation, J. Climate, 26, 2947–2956, doi:10.1175/JCLI-D-12-00506.1, 2013.

Hallberg, R. W. and Gnanadesikan, A.: On the role of eddies in determining the structure and response of the wind-driven Southern Hemisphere overturning: Results from the Modeling Eddies in the Southern Ocean (MESO) project, J. Phys. Oceanogr., 36, 2232–2252, 2006.

Huang, B. Y., Stone, P. H., Sokolov, A. P., and Kamenkovich, I. V.: The deep-ocean heat uptake in transient climate change, J. Climate, 16, 1352–1363, doi:10.1175/1520-0442-16.9.1352, 2003.

Huntingford, C., Cox, P. M., and Lenton, T. M.: Contrasting responses of a simple terrestrial ecosystem model to global change, Ecol. Model., 134, 41–58, 2000.

Kostov, Y., Armour, K. C., and Marshall, J.: Impact of the Atlantic meridional overturning circulation on ocean heat storage and transient climate change, Geophys. Res. Lett., 41, 2108–2116, doi:10.1002/2013GL058998, 2014.

Kuhlbrodt, T. and Gregory, J. M.: Ocean heat uptake and its consequences for the magnitude of sea level rise and climate change, Geophys. Res. Lett., 39, L18608, doi:10.1029/2012GL052952, 2012.

Kuhlbrodt, T., Gregory, J. M., and Shaffrey, L. C.: A process-based analysis of ocean heat uptake in an AOGCM with an eddy-permitting ocean component, Clim. Dynam., 45, 3205–3226, doi:10.1007/s00382-015-2534-0, 2015.

Landerer, F. W., Jungclaus, J. H., and Marotzke, J.: Regional dynamic and steric sea level change in response to the IPCC-A1B scenario, J. Phys. Oceanogr., 37, 296–312, doi:10.1175/JPO3013.1, 2007.

Lorbacher, K., Nauels, A., and Meinshausen, M.: Complementing thermosteric sea level rise estimates, Geosci. Model Dev., 8, 2723–2734, doi:10.5194/gmd-8-2723-2015, 2015.

Lowe, J. A. and Gregory, J. M.: Understanding projections of sea level rise in a Hadley Centre coupled climate model, J. Geophys. Res., 111, C11014, doi:10.1029/2005JC003421, 2006.

Marotzke, J.: Analysis of thermohaline feedbacks, in: Decadal climate variability, edited by: Anderson, D. L. T. and Willebrand, J., chap. Dynamics and Predictability, Springer-Verlag Berlin Heidelberg, 1996.

Marshall, J., Scott, J. R., Armour, K. C., Campin, J.-M., Kelley, M., and Romanou, A.: The ocean's role in the transient response of climate to abrupt greenhouse gas forcing, Clim. Dynam., 44, 2287–2299, doi:10.1007/s00382-014-2308-0, 2015.

Meehl, G. A., Stocker, T. F., Collins, W. D., Friedlingstein, P., Gaye, A. T., Gregory, J. M., Kitoh, A., Knutti, R., Murphy, J. M., Noda, A., Raper, S. C. B., Watterson, I. G., Weaver, A. J., and Zhao, Z.: Global climate projections, in: Climate Change 2007: The Physical Science Basis. Contribution of Working Group I to the Fourth Assessment Report of the Intergovernmental Panel on Climate Change, edited by: Solomon, S., Qin, D., Manning, M., Chen, Z., Marquis, M., Averyt, K. B., Tignor, M., and Miller, H. L., Cambridge University Press, 2007.

Melet, A. and Meyssignac, B.: Explaining the spread in global mean thermosteric sea level rise in CMIP5 climate models, J. Climate, 28, 9918–9940, doi:10.1175/JCLI-D-15-0200.1, 2015.

Merrifield, M. A., Thompson, P. R., and Lander, M.: Multidecadal sea level anomalies and trends in the western tropical Pacific, Geophys. Res. Lett., 39, L13602, doi:10.1029/2012GL052032, 2012.

Mikolajewicz, U. and Voss, R.: The role of the individual air-sea flux components in CO_2-induced changes of the ocean's circulation and climate, Clim. Dynam., 16, 627–642, 2000.

Morrison, A. K., Saenko, O. A., Hogg, A. M., and Spence, P.: The role of vertical eddy transport in Southern Ocean heat uptake, Geophys. Res. Lett., 40, 5445–5450, doi:10.1002/2013GL057706, 2013.

Morrison, A. K., Griffies, S. M., Winton, M., Anderson, W. G., and Sarmiento, J. L.: Mechanisms of Southern Ocean heat uptake and transport in a global eddying climate model, J. Climate, 29, 2059–2075, doi:10.1175/JCLI-D-15-0579.1, 2016.

Palanisamy, H., Meyssignac, B., Cazenave, A., and Delcroix, T.: Is anthropogenic sea level fingerprint already detectable in the Pacific Ocean?, Environ. Res. Lett., 10, 084024, doi:10.1088/1748-9326/10/8/084024, 2015.

Palter, J. B., Griffies, S. M., Samuels, B. L., Galbraith, E. D., Gnanadesikan, A., and Klocker, A.: The deep ocean buoyancy budget and its temporal variability, J. Climate, 27, 551–573, doi:10.1175/JCLI-D-13-00016.1, 2014.

Pardaens, A. K., Gregory, J. M., and Lowe, J. A.: A model study of factors influencing projected changes in regional sea level over the 21st century, Clim. Dynam., 36, 2015–2033, doi:10.1007/s00382-009-0738-x, 2011.

Perrette, M., Landerer, F., Riva, R., Frieler, K., and Meinshausen, M.: A scaling approach to project regional sea level rise and its uncertainties, Earth Syst. Dynam., 4, 11–29, doi:10.5194/esd-4-11-2013, 2013.

Rahmstorf, S. and Ganapolski, A.: Long-term global warming scenarios computed with an efficient coupled climate model, Clim. Change, 43, 353–367, 1999.

Rahmstorf, S. and Willebrand, J.: The role of temperature feedback in stabilizing the thermohaline circulation, J. Phys. Oceanogr., 25, 787–805, doi:10.1175/1520-0485(1995)025<0787:TROTFI>2.0.CO;2, 1995.

Roberts, C. D., Calvert, D., Dunstone, N., Hermanson, L., Palmer, M. D., and Smith, D.: On the drivers and predictability of seasonal-to-interannual variations in regional sea level, J. Climate, 29, 7565–7585, doi:10.1175/JCLI-D-15-0886.1, 2016.

Rugenstein, M. A. A., Winton, M., Stouffer, R. J., Griffies, S. M., and Hallberg, R.: Northern high-latitude heat budget decomposition and transient warming, J. Climate, 26, 609–621, doi:10.1175/JCLI-D-11-00695.1, 2013.

Russell, G. L., Gornitz, V., and Miller, J. R.: Regional sea-level changes projected by the NASA/GISS atmosphere-ocean model, Clim. Dynam., 16, 789–797, doi:10.1007/s003820000090, 2000.

Saenko, O. A., Yang, D., Gregory, J. M., Spence, P., and Myers, P. G.: Separating the influence of projected changes in air temperature and wind on patterns of sea level change and ocean heat content, J. Geophys. Res., 120, 5749–5765, doi:10.1002/2015JC010928, 2015.

Santer, B. D., Wigley, T. M. L., Schlesinger, M. E., and Mitchell, J. F. B.: Developing climate scenarios from equilibrium GCM results, Tech. Rep. 47, MPI Hamburg, 1990.

Sausen, R., Barthel, K., and Hasselmann, K.: Coupled ocean-atmosphere models with flux corrections, Clim. Dynam., 2, 154–163, 1988.

Schmidt, G. A., Ruedy, R., Hansen, J. E., Aleinov, I., Bell, N., Bauer, M., Baue, S., Cairns, B., Canut, V., Cheng, Y., Genio, A. D., Faluvegi, G., Friend, A. D., Hall, T. M., Hu, Y., Kelley, M., Kiang, N. Y., Koch, D., Lacis, A. A., Lerner, J., Lo, K. K., Miller, R. L., Nazarenko, L., Oinas, V., Perlwitz, J., Perlwitz, J., Rind, D., Romanou, A., Russell, G. L., Sato, M., Shindell, D. T., Stone, P. H., Sun, S., Tausnev, N., Thresher, D., and Yao, M.-S.: Present day atmospheric simulations using GISS Model E: Comparison to in-situ, satellite and reanalysis data, J. Climate, 19, 153–192, 2006.

Sen Gupta, A. and England, M. H.: Evaluation of Interior Circulation in a High-Resolution Global Ocean Model. Part I: Deep and Bottom Waters, J. Phys. Oceanogr., 34, 2592–2614, doi:10.1175/JPO2651.1, 2004.

Sen Gupta, A., Jourdain, N. C., Brown, J. N., and Monselesan, D.: Climate drift in the CMIP5 models, J. Climate, 26, 8597–8615, doi:10.1175/JCLI-D-12-00521.1, 2013.

Slangen, A. B. A., Carson, M., Katsman, C. A., van de Wal, R. S. W., Köhl, A., Vermeersen, L. L. A., and Stammer, D.: Projecting twenty-first century regional sea-level changes, Climatic Change, 124, 317–332, doi:10.1007/s10584-014-1080-9, 2014.

Smith, R. S., Gregory, J. M., and Osprey, A.: A description of the FAMOUS (version XDBUA) climate model and control run, Geosci. Model Dev., 1, 53–68, doi:10.5194/gmd-1-53-2008, 2008.

Spence, P., Griffies, S. M., England, M. H., Hogg, A. M., Saenko, O. A., and Jourdain, N. C.: Rapid subsurface warming and circulation changes of Antarctic coastal waters by poleward shifting winds, Geophys. Res. Lett., 41, 4601–4610, doi:10.1002/2014GL060613, 2014.

Stammer, D., Agarwal, N., Herrmann, P., Köhl, A., and Mechoso, C. R.: Response of a Coupled Ocean-Atmosphere Model to Greenland Ice Melting, Surv. Geophys., 32, 621–642, doi:10.1007/s10712-011-9142-2, 2011.

Stenchikov, G., Delworth, T. L., Ramaswany, V., Stouffer, R. J., Wittenberg, A., and Zeng, F.: Volcanic signals in oceans, J. Geophys. Res., 114, D16104, doi:10.1029/2008JD011673, 2009.

Stewart, A. L. and Thompson, A. F.: Eddy-mediated transport of warm Circumpolar Deep Water across the Antarctic Shelf Break, Geophys. Res. Lett., 42, 432–440, doi:10.1002/2014GL062281, 2015.

Stouffer, R. J.: Time scales of climate response, J. Climate, 17, 209–217, 2004.

Stouffer, R. J., Yin, J., Gregory, J. M., Dixon, K. W., Spelman, M. J., Hurlin, W., Weaver, A. J., Eby, M., Flato, G. M., Hasumi, H.,

Hu, A., Jungclaus, J., Kamenkovich, I. V., Levermann, A., Montoya, M., Murakami, S., Nawrath, S., Oka, A., Peltier, W. R., Robitaille, D. Y., Sokolov, A., Vettoretti, G., and Weber, N.: Investigating the Causes of the Response of the Thermohaline Circulation to Past and Future Climate Changes, J. Climate, 19, 1365–1387, doi:10.1175/JCLI3689.1, 2006.

Swingedouw, D., Rodehacke, C. B., Olsen, S. M., Menary, M., Gao, Y., Mikolajewicz, U., and Mignot, J.: On the reduced sensitivity of the Atlantic overturning to Greenland ice sheet melting in projections: a multi-model assessment, Clim. Dynam., 44, 3261–3279, doi:10.1007/s00382-014-2270-x, 2015.

Vaughan, D. G., Comiso, J. C., Allison, I., Carrasco, J., Kaser, G., Kwok, R., Mote, P., Murray, T., Paul, F., Ren, J., Rignot, E., Solomina, O., Steffen, K., and Zhang, T.: Observations: Cryosphere, in: Climate Change 2013: The Physical Science Basis. Contribution of Working Group I to the Fifth Assessment Report of the Intergovernmental Panel on Climate Change, edited by: Stocker, T. F., Qin, D., Plattner, G.-K., Tignor, M., Allen, S. K., Boschung, J., Nauels, A., Xia, Y., Bex, V., and Midgley, P. M., Cambridge University Press, doi:10.1017/CBO9781107415324.012, 2013.

Vizcaíno, M., Mikolajewicz, U., Jungclaus, J., and Schurgers, G.: Climate modification by future ice sheet changes and consequences for ice sheet mass balance, Clim. Dynam., 34, 301–324, doi:10.1007/s00382-009-0591-y, 2010.

Weijer, W., Maltrud, M. E., Hecht, M. W., Dijkstra, H. A., and Kliphuis, M. A.: Response of the Atlantic Ocean circulation to Greenland Ice Sheet melting in a strongly-eddying ocean model, Geophys. Res. Lett., 39, L09606, doi:10.1029/2012GL051611, 2012.

Winton, M., Griffies, S. M., Samuels, B. L., Sarmiento, J. L., and Frölicher, T. L.: Connecting changing ocean circulation with changing climate, J. Climate, 26, 2268–2278, doi:10.1175/JCLI-D-12-00296.1, 2013.

Winton, M., Anderson, W. G., Delworth, T. L., Griffies, S. M., Hurlin, W. J., and Rosati, A.: Has coarse ocean resolution biased simulations of transient climate sensitivity?, Geophys. Res. Lett., 41, 8522–8529, doi:10.1002/2014GL061523, 2014.

Xie, P. and Vallis, G. K.: The passive and active nature of ocean heat uptake in idealized climate change experiments, Clim. Dynam., 38, 667–684, doi:10.1007/s00382-011-1063-8, 2012.

Yang, D. and Saenko, O. A.: Ocean heat transport and its projected change in CanESM2, J. Climate, 25, 8148–8163, doi:10.1175/JCLI-D-11-00715.1, 2012.

Yin, J.: Century to multi-century sea level rise projections from CMIP5 models, Geophys. Res. Lett., 39, L17709, doi:10.1029/2012GL052947, 2012.

Yin, J., Schlesinger, M. E., and Stouffer, R. J.: Model projections of rapid sea-level rise on the northeast coast of the United States, Nat. Geosci., 2, 262–266, doi:10.1038/NGEO462, 2009.

Yin, J., Griffies, S. M., and Stouffer, R. J.: Spatial Variability of Sea Level Rise in Twenty-First Century Projections, J. Climate, 23, 4585–4607, doi:10.1175/2010JCLI3533.1, 2010.

Yin, J., Overpeck, J. T., Griffies, S. M., Hu, A., Russell, J. L., and Stouffer, R. J.: Different magnitudes of projected subsurface ocean warming around Greenland and Antarctica, Nat. Geosci., 4, 524–528, doi:10.1038/NGEO1189, 2011.

Zhang, X. and Church, J. A.: Sea level trends, interannual and decadal variability in the Pacific Ocean, Geophys. Res. Lett., 39, L21701, doi:10.1029/2012GL053240, 2012.